Timing and tectonic setting of tin mineralization in southern Myanmar: constraints from cassiterite and wolframite U–Pb ages

Qiang Zhang[1], Kui-Dong Zhao[1], Wen-Qian Li[2], Martin R. Palmer[3], Shao-Yong Jiang[1], Hai Jiang[1], Wei Zhang[1], Di Zhang[1], Amjad Hussain[1]

1 State Key Laboratory of Geological Processes and Mineral Resources, Collaborative Innovation Center for Exploration of Strategic Mineral Resources, School of Earth Resources, China University of Geosciences, Wuhan 430074, China

2 Key Laboratory of Mineralogy and Metallogeny, Guangzhou Institute of Geochemistry, Chinese Academy of Sciences, Guangzhou 510640, China

3 School of Ocean and Earth Sciences, University of Southampton, National Oceanography Centre, Southampton SO14 3ZH, UK

Abstract

The southern Myanmar tin ore district is an important part of the well-known Southeast Asia tin belt (SATB), and hosts numerous economically important primary tin-tungsten ore deposits. However, the timing of formation of these deposits is unclear due to the scarcity of robust age data. The tectonic setting of tin mineralization in this area also needs to be further constrained. Most of the primary tin-tungsten ore deposits in southern Myanmar are typical hydrothermal quartz vein–type, with cassiterite and wolframite as the main ore minerals. Here, we present in situ U–Pb ages of cassiterite and wolframite from nine granite-related hydrothermal Sn–W deposits in southern Myanmar. Cassiterite samples from the Hermyingyi, Thitkhatoe, Thaling Taung, Kalonta, Taungphila, Pagaye, Bawapin, Kanbauk, and Letha Taung deposits yield common lead-corrected weighted mean 206Pb/238U ages of 61.6 ± 0.8 Ma, 61.9 ± 0.6 Ma, 60.4 ± 0.9 Ma, 63.0 ± 0.6 Ma, 62.9 ± 0.6 Ma, 69.5 ± 0.5 Ma, 63.6 ± 0.6 Ma, 61.3 ± 0.6 Ma,

and 84.9 ± 0.5 Ma, respectively. Wolframite samples collected from these deposits also yield consistent ages with the cassiterite samples. These ages, combined with available tin mineralization ages from other deposits in the western part of the SATB, define three epochs of Sn metallogeny related to three contrasting geodynamic settings: (1) Early Cretaceous (~ 125–110 Ma) mineralization is related to post-collision slab break-off after collision between the West Burma terrane and the Sibumasu-Tengchong terrane; (2) Late Cretaceous to Paleocene (~ 90–60 Ma) mineralization developed in an Andean-type accretionary setting during subduction of the Neo-Tethys oceanic lithosphere; (3) Early Eocene (~ 50–40 Ma) mineralization may have formed in a post-collision setting after the India-Asia collision.

Keywords: Cassiterite, Wolframite, U–Pb geochronology, Tin deposits, Southern Myanmar, Southeast Asia tin belt

Introduction

The global distribution of tin ore deposits is well characterized (Lehmann 1990), with most tin ore deposits distributed in four belts (or provinces) within larger granite belts: the Southeast Asia tin belt, the South China tin province, the Bolivian tin belt, and the Erzgebirge-Iberia-Cornwall tin belt. These four regions account for about 85% of the cumulative historic tin mine output and two-thirds of current global tin reserves. In addition, more than 99% of the global tin production is from ore deposits directly (primary deposits) or indirectly (placers) related to granitic rocks, i.e., granites and their volcanic and subvolcanic equivalents (Lehmann 2020). Primary tin ore deposits are spatially associated with differentiated granites and are interpreted to be of magmatic-hydrothermal origin (Heinrich 1990; Lehmann 2020). However, the tectonic controls on the formation of these tin belts or provinces are less well constrained (Mithchell

and Garson 1981; Mlynarczyk and Williams-Jones 2005; Romer and Kroner 2016; Mao et al. 2019).

The Southeast Asian tin belt (SATB) is the largest tin province in the world, containing over half of the world's tin reserves and historically accounting for 40–45% share of the world's total tin production (Schwartz et al. 1995; Lehmann 2020). The belt extends from Yunnan in China through Myanmar and Thailand, via Malaysia, to Indonesia, over a distance of 2800 km and a width of 400 km (Beckinsale 1979; Schwartz et al. 1995) (Fig. 1a). Primary tin deposits in the SATB occur mainly along the eastern Tethyan tectonic domain (Mitchell 1979; Zaw et al. 2014). Myanmar is located at the southern edge of the Himalayan Syntaxis and represents a southward extension of the Tibetan-Himalayan orogeny (Fig. 1a), and was a major tin and tungsten producer pre-World War II. It experienced considerable depression during the past 60 years (Schwartz et al. 1995), but in recent years, Myanmar tin production has greatly increased owing to the newly discovered tin mining district at Man Makhsan in the Wa State. This made Myanmar the world's third-largest producer of tin after China and Indonesia in 2014 (Gardiner et al. 2015b; Htun et al. 2017). The southern Myanmar tin ore district lies in the western range of the SATB, and hosts numerous primary large- and medium-size tin-tungsten deposits (Htun et al. 2017) (Fig. 1b); some of which have been mined for over 100 years. Studies of the tin mineralization in this region have focused mainly on the granites, with fewer studies of the ore genesis within the deposits (Zaw 1984; Lehmann et al. 1994; Li et al. 2018a, 2018b, 2019b, 2020a; Myint et al. 2017, 2018; Paik 2017; Jiang et al. 2019; Mao et al. 2020). Nevertheless, better understanding the timing and genesis of tin mineralization in southern Myanmar is critical for understanding metallogenesis in the SATB and the Tethyan metallogenic province as a whole (Hou and Zhang 2015).

Previous studies have shown that Sn–W deposits and occurrences in this area are spatially and genetically associated with Cretaceous-Eocene granite intrusions (Hutchison and

Taylor 1978; Zaw 1990), which intruded metasedimentary rocks of the Slate Belt. However, the timing and tectonic setting of tin mineralization in southern Myanmar are debated due to the lack of reliable mineralization ages. The association between the local Tethyan tectonic evolution and formation of the tin deposits urgently needs to be constrained by robust age data for tin mineralization. Cassiterite (SnO_2) has a tetragonal lattice structure with Sn cations in sixfold coordination with oxygen. It often contains > 10 ppm U, with relatively low common Pb, and has the ability to retain U and radiogenic Pb (Gulson and Jones 1992; Yuan et al. 2008), making it a robust U–Pb geochronometer for direct dating of tin mineralization (Yuan et al. 2011; Li et al. 2016; Zhang et al. 2017b; Neymark et al. 2018). Wolframite [$(Fe,Mn)WO_4$] is an isomorphous solid-solution series of two end members: ferberite ($FeWO_4$) and hubnerite ($MnWO_4$). It may also contain relatively high U contents and variable contents of common Pb (Luo et al. 2019; Yang et al. 2020). Recently, great progress has been made on in situ cassiterite and wolframite U–Pb dating, and accurate mineralization ages have been obtained in many typical Sn–W deposits (Zhang et al. 2017b; Deng et al. 2019; Moscati and Neymark 2020; Yang et al 2020).

Here, we present U–Pb dating results on cassiterite and wolframite collected from nine representative primary tin ore deposits in southern Myanmar. These data allow us to constrain the timing of these tin deposits, and provide important information regarding the genetic link between Tethyan tectonic evolution and tin mineralization.

Geological background

The Mesozoic-Cenozoic geology of Southeast Asia is dominated by the subduction and accretion of a series of fragments of oceanic crust and island arc terranes that rifted away from the northwestern Gondwana supercontinent margin at different periods in the Phanerozoic, and eventually sutured onto the South China Block (Hutchison 1993; Hall 2012; Metcalfe 2013).

This history of rifting and suturing records the staged closing of the Tethys Ocean, rendering much of Southeast Asia a collage of continental terranes separated by suture zones (Fig. 1).

Two primary subduction and collisional events dominate the Mesozoic-Cenozoic geological history of Myanmar. (1) The earlier Late Triassic closure of Paleo-Tethys involved the collision of the Sibumasu terrane with the Indochina terrane, and resulted in the Indosinian orogeny (Metcalfe 2011; Sone and Metcalfe 2008; Gardiner et al. 2016b). (2) The Cretaceous-Eocene eastward subduction of the Neo-Tethys oceanic plate resulted in the formation of the Wuntho-Popa magmatic Arc (Popa-Loimye Arc) in the West Burma terrane. The final closure of the Neo-Tethys Ocean was sutured in the Late Eocene (Mitchell et al. 2012; Acharyya 2015), forming the Indo-Burma ranges between the India plate and the West Burma terrane. In addition, the oblique convergence and collision between the Indian and Eurasian plates led to strike-slip faults, such as the dextral Sagaing Fault System (Fig. 1a). These faults extensively disrupted the original orogenic architecture of Myanmar, producing secondary orogenic collages or terranes, such as the Mogok Metamorphic Belt (Mitchell et al. 2012).

Multiple tectono-magmatic-hydrothermal events occurred throughout this time and led to the formation of the Southeast Asian granite belt that can be divided into three provinces based on their ages, mineralogical, geochemical affinities, and tectonic setting (Fig. 1a) (Mitchell 1977; Hutchison and Taylor 1978; Cobbing et al. 1986; Searle et al. 2012). The Western Granite Province (WGP) extends from west Yunnan in China through central Myanmar to peninsular Thailand, containing a mixture of I- and S-type granites with mainly Cretaceous to Cenozoic ages (Cobbing et al. 1986; Zaw 1990; Barley et al. 2003). The Main Granite Province (MGP) runs through western Yunnan, eastern Myanmar, western Thailand, and western Peninsular Malaysia, and consists predominantly of S-type granites with mainly Triassic ages (Charusiri et al. 1993; Ng et al. 2015a, 2015b). The Eastern Granite Province (EGP) outcrops in northern Laos, central-eastern Thailand, and eastern Malaysia and is

dominantly composed of I-type granites with Permo-Triassic ages (Ng et al. 2015a, b). Tin mineralization occurred in all three granite provinces, but the major tin deposits are focused in and around the S-type granites of the WGP and MGP. Sn-bearing granites in the WGP intruded Carboniferous to Early Permian metasedimentary and sedimentary sequences of the Slate Belt that comprises the sediments and low-grade metasediments of the Lebyin, Mawchi, and Mergui groups in Myanmar and the Kaeng Krachan group in Thailand.

Deposit geology and samples

The southern Myanmar tin ore district is principally focused in a north–south trending belt that extends from east of Yangon southwards along the Myeik Archipelago (Fig. 1b). Primary tin mineralization occurs mainly as cassiterite quartz veins within the country rock and the cupolas of the granite intrusions. The principal tin-producing areas are located around Dawei and Myeik towns, with much of the historical production from placers (Htun et al. 2017). This tin metallogenic district is also rich in tungsten that is commonly found spatially associated with tin as wolframite and rare scheelite (Htun et al. 2019).

Hermyingyi Sn–W deposit

The Hermyingyi deposit (14° 15′ N, 98° 21′ E) is situated about 40 km northeast of Dawei Town, Tennasserim Division. It is a typical quartz vein–type Sn–W deposit and has been mined for over 100 years. The deposit contains about 700,000 tons of ore reserve at a grade of 0.38% (Htun et al. 2017). The mine area is underlain by the Upper Carboniferous to Lower Permian metasedimentary rocks of the Mergui group that is intruded by the Hermyingyi biotite granite (Fig. 2) (Jiang et al. 2017, 2019). More than 60 quartz-wolframite-cassiterite main and branch veins have been explored and mined. These veins strike N-S with steep easterly dips of 80°–85°. The veins vary from several cm to 2 m in thickness and crosscut the granite and country

rocks (Fig. 3a-b). Hydrothermal alteration is well-developed near the veins, including several cm thick envelopes of greisenization and silicification. The ore minerals in the veins mainly include wolframite and cassiterite, with associated sulphides (pyrite, sphalerite, galena, and molybdenite). In general, sulfide minerals were precipitated after cassiterite and wolframite. Both the cassiterite sample HMG-10 and wolframite sample HMG-4 were collected from quartz veins within the granite. HMG-10 comprises large, dark brown cassiterite crystals intergrown with wolframite and quartz (Fig. 4a). Cassiterite is transparent to translucent and most show oscillatory zoning (Fig. 4b). HMG-4 consists of massive black wolframite crystals and minor quartz (Fig. 5a-b).

Thitkhatoe Sn–W deposit

The Thitkhatoe Sn–W deposit (14° 15′ N, 98° 20′ E) lies ~ 2 km to the northwest of the Hermyingyi deposit, and is underlain by the same Mergui group metasedimentary rocks found at Hermyingyi. Sn–W quartz veins strike approximately N-S and penetrate the country rock. The vein mineralogy and orientation are also similar with those in the Hermyingyi Sn–W deposit. Cassiterite sample TKT-2 and wolframite sample TKT-3 were chosen from two quartz veins. TKT-2 is composed of brown cassiterite grains, massive quartz, and later sulfide minerals (Fig. 4c). Cassiterite occurs as euhedral to subhedral grains (0.5–4 mm) (Fig. 4d). Wolframite crystals in sample TKT-3 are intergrown with quartz (Fig. 5c-d).

Thaling Taung Sn–W deposit

Samples TLT-6 and TLT-8 were collected from the Thaling Taung deposit (14° 16′ N, 98° 20′ E), located ~ 48 km northeast of Dawei Town. The deposit exploits quartz-cassiterite-wolframite veins which cut the biotite granite and Mergui group (Fig. 3c). Hydrothermal Sn–W quartz veins are roughly N-S-trending and range from several cm to 1 m in width.

Cassiterite, wolframite and minor pyrite and molybdenite are present within these quartz veins. The cassiterite in sample TLT-6 is from the quartz vein and is dark brown in color (Fig. 4e). The cassiterite is euhedral to subhedral (0.5–3 mm), while quartz occurs as anhedral grains (Fig. 4f). Wolframite crystals in the sample TLT-8 are typically black, euhedral to subhedral with lengths up to 4 mm (Fig. 5e-f).

Kalonta Sn–W deposit

The Kalonta deposit (14° 17′ N, 98° 16′ E) is situated ~ 60 km to the NE of Dawei Town. Both primary ores and thick placer deposits are present in the mine. The cassiterite and wolframite were derived from numerous Sn–W quartz veins which cut the underlying sedimentary rocks of the Mergui Group. Sample KLT-3 is dominated by cassiterite crystals surrounded by abundant quartz (Fig. 4g-h). Sample TLT-7 contains large black wolframite grains intergrown with cassiterite and quartz (Fig. 5g-h).

Taungphila Sn–W deposit

The Sn–W mineralization in the Taungphila deposit (14° 13′ N, 98° 21′ E) is spatially associated with a granite pluton. The pluton is a medium- to fine-grained monzogranite composed of K-feldspar, plagioclase, quartz, biotite, muscovite and accessory minerals (Jiang et al. 2017). The area is also underlain by the sedimentary rocks of Mergui group. Abundant quartz veins from several mm to over 30 cm wide are hosted in the monzogranite. Cassiterite and wolframite mineralization mainly developed in the quartz veins, with minor disseminated mineralization in the greisenized granite. Sample TPL-5 was collected from the contact zone between the quartz vein and greisen (Fig. 4i). The cassiterite grains are dark brown, have a euhedral texture, and are surrounded by muscovite (Fig. 4j). In sample TPL-6, black, lath-shaped, wolframite with brown cassiterite coexists with quartz (Fig. 5i-j).

Pagaye Sn–W deposit

The Pagaye deposit (14° 05′ N, 98° 19′ E) is a Sn–W lode mine located ~ 19 km east of Dawei Town. This deposit contains about 6000 tons of Sn + W metal reserve. The Mergui group is intruded by biotite granite, pegmatites, and cut by quartz veins, with the latter striking N35° W and S35° E and dipping 80° NNE. The vein zone is 18 m wide in the north, 24 m in the southern end, and 36 m in the middle. All the veins are bordered by mica selvages. Pegmatitic stockworks are also present. Cassiterite and wolframite are the main ore minerals, with pyrite, chalcopyrite, sphalerite, galena, small quantities of scheelite, and fluorite also present. Samples for cassiterite and wolframite U–Pb dating were collected from a quartz vein within the granite. The PGY-2 sample consists of prominent brown cassiterite with muscovite and massive quartz (Fig. 4k). Most of the cassiterite occurs as zoned, euhedral crystals (Fig. 5l). Wolframite crystals from sample TLT-8 are enclosed by abundant quartz (Fig. 5k-l).

Bawapin Sn–W deposit

The Bawapin deposit (14° 09′ N, 98° 23′ E) is also a typical Sn–W lode mine and lies ~ 70 km northeast of Dawei Town. The quartz veins contain cassiterite and wolframite with accessory pyrite, chalcopyrite, sphalerite, galena, and molybdenite. Cassiterite sample BWP-9 and wolframite sample BWP-10 were collected for U–Pb dating from quartz veins. BWP-9 is dominated by brown cassiterite, wolframite, muscovite, and quartz crystals (Fig. 4m-n). BWP-10 is composed of large black wolframite embedded within massive quartz (Fig. 5m-n).

Kanbauk Sn–W deposit

The Kanbauk deposit (14° 34′ N, 98° 01′ E) is located ~ 90 km north of Dawei Town in a narrow valley surrounded by granite hills on the southern flank of the Heinz Basin. The mine area is ~ 500 m long by ~ 250 m wide and hosts at least 20 ore veins (Bender 1983). This

deposit contains about 1300 tons of Sn metal reserve. Both quartz vein–type and skarn-type ores occur at the contact zone of the granite and the Mergui group sedimentary rocks. The quartz veins vary from several cm to 0.5 m thick with an E-W strike and a steep dip to the south. The ore minerals consist of cassiterite, wolframite, and scheelite, with associated pyrite, chalcopyrite, galena, sphalerite, and bismuth. Samples KBK-7 and KBK-8 were chosen from the same quartz vein. Cassiterite sample KBK-7 comprises abundant brown cassiterite grains intergrown with quartz (Fig. 4o). Twining is a common feature of most cassiterite grains (Fig. 4p). The wolframite crystals in KBK-8 are massive, with a black color (Fig. 5o-p).

Letha Taung Sn–W deposit

The Letha Taung deposit (12° 14′ N, 98° 59′ E) is a typical Sn–W vein-type deposit in the Myeik district and is situated ~ 50 km northeast of Myeik Town. A biotite granite intruded the phyllites, slates, and quartzites of the Mergui group. Numerous quartz veins and stringers penetrated both the granite and sedimentary rocks (Fig. 3d), with the veins in the granite showing greisenized borders. Wolframite, cassiterite and minor pyrite, chalcopyrite, and bismuth developed in these veins. The cassiterite crystals in sample LTT-1 are up to 1.5 cm in length and are typically dark brown, euhedral, intergrown with quartz (Fig. 4q-r). In sample LTT-5, abundant euhedral to subhedral wolframite crystals are surrounded by quartz (Fig. 5q-r).

Analytical methods

LA-ICP-MS cassiterite U–Pb dating

Cassiterite-bearing samples were crushed to 500 μm and the cassiterite grains were hand-picked under a binocular microscope. The grains were then mounted in epoxy resin and polished to expose their interior. The mounts were examined under reflected light microscopy,

backscattered electron (BSE), and cathodoluminescence (CL) imaging to avoid inclusions and cracks during laser ablation.

Cassiterite U–Pb dating was performed at the State Key Laboratory of Geological Processes and Mineral Resources (GPMR), China University of Geosciences, using a Thermo iCAP Qc ICP-MS equipped with a RESOlution S-155 193 nm ArF excimer laser ablation system. Helium gas carrying the ablated sample aerosol was mixed with argon gas and a little nitrogen gas, and flowed into the ICP-MS. Prior to analysis, the LA-ICP-MS system was optimized using NIST SRM 612 ablated with a 50 μm spot size and 5 μm/s scan speed to ensure maximum signal intensity and low oxide formation. A cassiterite standard AY-4 was used as an external isotopic calibration standard. The U–Pb age of AY-4 was established by ID-TIMS as 158.2 ± 0.4 Ma (Yuan et al. 2011). Each set of eight analyses was followed by three measurements of AY-4 and one measurement of NIST SRM 612. Cassiterite grains were analyzed using a laser energy density of 3.5 J/cm^2, a spot size of 50 μm, and a laser pulse rate of 8 Hz. Each spot analysis consisted of 30 s background acquisition and 40 s data acquisition, and 60 s for cleaning the sample cell and plumbing lines. The isotopes were measured in time-resolved mode. For U–Pb dating, dwell times for each mass scan are 20 ms for ^{238}U, ^{232}Th, ^{208}Pb, ^{206}Pb, ^{204}Pb, and 40 ms for ^{207}Pb. Offline raw data reduction was performed using Iolite software for semi-quantitative calculation of trace element contents (Paton et al. 2011) and ICPMSDataCal software for U–Pb age calculation (Liu et al. 2010). Owing to the high content of common Pb in cassiterite, the ages are reported as lower intercept ages in the Tera–Wasserburg diagram (Tera and Wasserburg 1972). In order to compare with the lower intercept ages, the ^{207}Pb-corrected ^{206}Pb/^{238}U ages were also calculated using the common Pb composition corresponding to the two-stage model of Stacey and Kramers (1975). Concordia diagrams and weighted average ages with outlier rejection were calculated using Isoplot 4.0 software package (Ludwig 2012). Data uncertainties for isotopic ages are presented as 1σ.

LA-SF-ICP-MS wolframite U–Pb dating

Measurements of U, Th, and Pb isotopes in wolframite were conducted using a ThermoFisher Element XR SF-ICP-MS, coupled to a Geolas HD 193 nm ArF excimer laser ablation system at the Institute of Geology and Geophysics, Chinese Academy of Science, Beijing, following the procedures described by Yang et al. (2020). Helium and a little nitrogen were used as the carrier gas through the ablation cell and mixed with argon prior to introduction into the SF-ICP-MS. Prior to analysis, the LA-SF-ICP-MS system was optimized using NIST SRM 612 for maximum Pb, Th, and U sensitivity while satisfying low oxide production rates (ThO^+/Th^+ < 0.5%) and double-charged ions (Ca^{2+}/Ca^+ < 1.0%). The U+/Th+ ratio was in the range of 0.95–1.05. The isotopes ^{202}Hg, ^{204}Pb, ^{206}Pb, ^{207}Pb, ^{208}Pb, ^{232}Th, ^{235}U, and ^{238}U were analyzed by cycling of the electrostatic analyzer in the eScan mode, at a static magnetic mass. YGX-2113 wolframite was used as a primary U–Pb isotopic calibration standard which yielded an ID-TIMS concordia age of 160.9 ± 0.2 Ma (Yang et al. 2020). SHM huebnerite from the Sweet Home Mine, USA, was used as a secondary reference material for monitoring data reproducibility. In order to eliminate common Pb contamination, the sample surface was cleaned directly before each analysis by ablating a 90 μm spot for two pre-ablation pulses. Wolframite grains were analyzed using a laser energy density of 2.0 J/cm^2, a spot size of 50 μm, and a laser pulse rate of 8 Hz. Each spot analysis consisted of a 15 s background and 45 s sample data acquisition. For U–Pb isotope analyses, dwell times for each mass scan are 15 ms for ^{206}Pb and ^{238}U, 2 ms for ^{202}Hg and ^{204}Pb, 10 ms for ^{208}Pb and ^{232}Th, and 30 ms for ^{207}Pb. Raw data were reduced off-line using the Iolite program for semi-quantitative calculation of Pb, Th, and U contents (Paton et al. 2011) and Glitter software for U–Pb age calculation (Griffin et al. 2008). The lower intercept ages in the Tera-Wasserburg (TW) diagram were used for dating the wolframite samples (Tera and Wasserburg 1972). Weighted $^{206}Pb/^{238}U$ mean

ages for each spot were also calculated using the ^{207}Pb correction of common Pb. The common Pb composition of Stacey and Kramers' (1975) two-stage crustal Pb model was used for this correction. The data were plotted using Isoplot 4.0 software (Ludwig 2012). The secondary standard wolframite SHM yielded a TW lower intercept age of 26.0 ± 0.3 Ma (1σ, *n* = 52, MSWD = 0.5) in this study, in agreement with an ID-TIMS age of 25.7 ± 0.3 Ma (Romer and Luders 2006).

Results

Cassiterite U–Pb dating

Most of the cassiterite grains studied here are zoned and show obvious oscillatory zonation under CL (Fig. 6). U–Th–Pb concentration data and isotopic results of cassiterite from each deposit are given in the Electronic Supplementary Material (ESM Table S1) and the TW plots shown in Fig. 7. The sample names, locations, and isotopic ages for the 9 cassiterite samples are also summarized in Table 1. Cassiterite samples from the Hermyingyi, Thitkhatoe, Thaling Taung, Kalonta, Taungphila, Pagaye, Bawapin, Kanbauk, and Letha Taung deposits yield common lead-corrected weighted mean ^{206}Pb/^{238}U ages of 61.6 ± 0.8 Ma, 61.9 ± 0.6 Ma, 60.4 ± 0.9 Ma, 63.0 ± 0.6 Ma, 62.9 ± 0.6 Ma, 69.5 ± 0.5 Ma, 63.6 ± 0.6 Ma, 61.3 ± 0.6 Ma, and 84.9 ± 0.5 Ma, respectively. It should be noted that in all cases, the TW lower intercept ages are within errors of the ^{207}Pb-corrected ^{206}Pb/^{238}U ages.

The U and Th concentrations range from 1.7 to 261 ppm and 0.01 to 0.14 ppm, respectively. Total Pb concentrations range from 0.03 to 52 ppm. Sample PGY-2 from the Pagaye deposit has the highest U concentrations with a median U value of 81 ppm. Cassiterite samples TKT-2, BWP-9, KBK-7, and LTT-1 also have relatively high U concentrations with median U values of 36.8, 54.0, 43.3, and 55.7 ppm, respectively. Sample HMG-10 from the Hermyingyi deposit has the lowest median U value of 9.6 ppm.

Wolframite U–Pb dating

U–Th–Pb concentration data and isotopic ages of wolframite samples from nine Sn–W deposits are presented in ESM Table S2. U–Pb isotope data are illustrated on TW plots (Fig. 8). The TW lower intercept ages and the ^{207}Pb-corrected ^{206}Pb/^{238}U ages for the wolframite samples are listed in Table 1. Wolframites from the Hermyingyi, Thitkhatoe, Thaling Taung, Kalonta, Taungphila, Pagaye, Bawapin, Kanbauk, and Letha Taung deposits yield ^{207}Pb-corrected weighted mean ^{206}Pb/^{238}U ages of 60.9 ± 1.3 Ma, 64.3 ± 2.9 Ma, 62.4 ± 0.8 Ma, 64.2.0 ± 2.2 Ma, 64.5 ± 1.1 Ma, 68.4 ± 2.7 Ma, 63.4 ± 0.8 Ma, 62.4 ± 2.4 Ma, and 85.2 ± 2.2 Ma, respectively. These ages are consistent with the cassiterite ages from the same deposits.

Contents of U and Th in the wolframite samples range between 0.1 and 210 ppm, and 0.01 and 22.6 ppm, respectively. Total Pb concentrations range from 0.02 to 15.5 ppm except for sample TKT-3. TKT-3 from the Thitkhatoe deposit has unusually high Pb concentrations (from 1.0 to 4240 ppm). Sample TKT-3, TLT-8, and TPL-6 have relatively high U concentrations with median U values of 64.9, 41.8, and 67.4 ppm, respectively. Sample KBK-8 from the Kanbauk deposit has the lowest median U value of 0.4 ppm.

Discussion

Interpretation and evaluation of cassiterite and wolframite ages

Precise and accurate mineralization age data from an ore deposit are a prime prerequisite for understanding ore genesis and geotectonic settings. Because Sn–W deposits are commonly associated with granitic rocks, zircon in granite and co-existing minerals (e.g., mica, xenotime) or the associated molybdenite are often used to determine the timing of Sn–W mineralization. Interpretation of these data as mineralization ages, however, assumes that these minerals precipitated at the same time as the Sn–W ore, and that the original geochronological information contained within them has not been altered by subsequent thermal events. In

contrast, in situ U–Pb isotopic dating of cassiterite and wolframite can provide direct constraints on Sn–W mineralization ages.

In the Hermyingyi deposit, cassiterite and wolframite U–Pb isotope data yield 207Pb-corrected weighted average $^{206}Pb/^{238}U$ ages of 61.6 ± 0.8 and 60.9 ± 1.3 Ma (Table 1), respectively. The Hermyingyi granite has a SHRIMP zircon U–Pb age of 61.7 ± 1.3 Ma (Mitchell et al. 2012). Jiang et al. (2017) reported a LA-ICPMS zircon U–Pb age of 70.0 ± 0.4 Ma for the Hermyingyi granite. However, Li et al. (2018a) presented a LA-ICP-MS zircon U–Pb age of 61.6 ± 0.5 Ma for the granite. Jiang et al. (2019) also recorded a Re–Os isochron age of 68.4 ± 2.5 Ma for the molybdenite, which was interpreted as the mineralization age. The cassiterite and wolframite U–Pb ages obtained by us are younger than the LA-ICP-MS zircon U–Pb age of 70.0 ± 0.4 and the molybdenite Re–Os isochron age of 68.4 ± 2.5 Ma (Jiang et al. 2017, 2019) (Fig. 9). In this deposit, most of the ore veins crosscut the granite (Fig. 3a-b), indicating that the mineralization should be later than the emplacement of the granite. The cassiterite age and the wolframite age came from different laboratories by different methods. Therefore, we conclude that the weighted average age of ~ 61 Ma is most likely to represent the Sn–W mineralization age of the Hermyingyi deposit.

Cassiterite and wolframite samples in the Taungphila Sn–W deposit yield consistent ^{207}Pb-corrected weighted average $^{206}Pb/^{238}U$ age of 62.9 ± 0.6 and 62.5 ± 1.1 Ma (Table 1), respectively, but they are also younger than the zircon U–Pb age of 68.9 ± 1.8 Ma of the granite (Jiang et al. 2017) (Fig. 9). In the Kalonta Sn–W deposit, the ^{207}Pb-corrected weighted average $^{206}Pb/^{238}U$ ages of 63.0 ± 0.6 and 64.2 ± 2.2 Ma (Table 1) for the cassiterite and wolframite samples overlap within error and are in good agreement with the cassiterite U–Pb age of 64.6 ± 3.9 Ma reported by Li et al. (2018b). The U–Pb ages of 63.6 ± 0.6 and 63.4 ± 0.8 Ma (Table 1) for the cassiterite and wolframite samples from the Bawapin Sn–W deposit are slightly older than the cassiterite U–Pb ages of the 60.7 ± 2.5 Ma (Li et al. 2018b). Overall, the pairs of

associated cassiterite and wolframite samples from the other five Sn–W deposits in southern Myanmar yield consistent ^{207}Pb-corrected weighted average ^{206}Pb/^{238}U ages that overlap within error (Table 1).

Timing of Sn–W mineralization in the western SATB

The tin ore deposits in the western SATB are hosted in the Tengchong and west Sibumasu terranes and form an elongated north–south trending tin mineralization belt (Fig. 10). Details of the major Sn–W deposits in this tin belt are summarized in Table 2. The Tengchong- Lianghe tin belt in the Tengchong terrane contains two large tin deposits (Xiaolonghe and Lailishan), five medium-sized tin deposits, and nearly a hundred reported mineralized occurrences (Hou et al. 2007). Three periods of tin metallogenesis associated with felsic magmatism events have been identified in this area: (1) Early Cretaceous (~ 120 Ma) skarn-type tin bearing polymetallic mineralization (Chen et al. 2014; Cao et al. 2017a); (2) Late Cretaceous (~ 70 Ma) vein/ greisen-type Sn–W mineralization (Ma et al. 2013; Chen et al. 2014, 2015; Cao et al. 2016; Zhou et al. 2017; Wu et al. 2019); and (3) Eocene (~ 50 Ma) vein/ greisen-type Sn–W mineralization (Chen et al. 2014, 2015, 2018; Wu et al. 2019). In the west Sibumasu terrane, primary Sn–W deposits and occurrences are spatially and genetically associated with the Cretaceous to Eocene granite, granitic pegmatites, and aplite dykes of the WGP (Mitchell 1977; Beckinsale 1979; Cobbing et al. 1986; Zaw 1990; Schwartz et al. 1995; Gardiner et al. 2015a, 2016a, 2018; Crow and Zaw 2017; Mitchell 2018). Based on the published LA-ICP-MS zircon U–Pb data, the earliest tin mineralization event (120–107 Ma) is recorded by the Sn–W mineralization in the Mawpalaw Taung area, ~ 80 km south of Mawlamyine (Paik 2017). Whereas, the granitic magmatic events related to the Kuntabin, Hermyingyi, Taungphila, Wagone, and Yadanabon Sn mineralization have been dated at 90.1 Ma, 61.4–70.5 Ma, 68.8 Ma, 61.4 Ma, and 50.3 Ma respectively (Pickard et al. 1996; Mitchell et al. 2012; Gardiner et

al. 2016a; Jiang et al. 2017; Li et al. 2018a; Mao et al. 2020). In the Mawchi deposit, previously reported LA-ICP-MS zircon U–Pb and biotite Ar–Ar dates, integrated with molybdenite Re–Os model ages, suggest that the granite and corresponding tin mineralization occurred at ~ 42 Ma (Myint et al. 2017, 2018).

The cassiterite LA-ICP-MS U–Pb and wolframite LA-SF-ICP-MS U–Pb dates (Table 1) of nine Sn–W deposits presented here suggest that tin mineralization in Dawei and Myeik mainly formed between 85 and 60 Ma (Fig. 9). Together with other published tin mineralization ages (Table 2), we argue that there were at least three distinct Sn metallogenic events in the western SATB (Fig. 11): (1) the Early Cretaceous (~ 125–110 Ma) Sn metallogenic event generated the Jiaojiguan and Tieyaoshan deposit in the Tengchong terrane and the Mawpalaw Taung deposit in the west Sibumasu terrane, respectively; (2) the Late Cretaceous–Early Paleocene (~ 90–60 Ma) Sn metallogenic event developed the Xiaolonghe-Dasongpo and Xinqi deposit in the Tengchong terrane and numerous tin deposits (e.g., Kuntabin, Hermyingyi) in the west Sibumasu terrane; (3) the Early Eocene (~ 50–40 Ma) Sn metallogenic event is represented by the large Lailishan deposit in the Tengchong terrane and the Mawchi deposit in the west Sibumasu terrane. Moreover, these three periods of events are almost entirely coincident with zircon U–Pb ages of granite intrusions in the WGP (Fig. 11a-b), indicating a close genetic relationship between tin mineralization and the felsic magmatism in the western SATB.

Tectonic setting for tin mineralization in the western SATB

The modern Eastern Tethyan margin comprises several continental terranes that amalgamated to the southern margin of Eurasia during the closure of the various Tethys oceans after rifting and separation from northern Gondwana (Metcalfe 2011; Barber et al. 2011). The tectonic processes and magmatic histories of the Mesozoic to Cenozoic Eastern Tethyan margin within

Southeast Asia are complex, and a variety of tectonic models for the margin have been proposed (Mitchell 1979, 1986; Zaw 1990; Cobbing et al. 1992; Barber et al. 2017; Mitchell 2018; Gardiner et al. 2018; Lin et al. 2019). For example, some studies suggest that the Sibumasu terrane and the West Burma terrane are effectively a single crustal terrane termed the "Greater Sibumasu" which is bounded on the west by the Kalaymyo ophiolite belt (Morley and Searle 2017; Gardiner et al. 2018). However, others argued that the West Burma terrane is not a part of the Sibumasu terrane, but aggregated during the Tethys ocean basin closure (Metcalfe 2013; Ridd 2016, 2017; Mitchell 2018; Lin et al. 2019). The most critical debate among these models is whether there was subduction and closure of the Meso-Tethys Ocean in Southeast Asia, i.e., whether the Meso-Tethys suture zone extends southeastward into western Yunnan, China, and Myanmar. The Meso-Tethys suture is best exposed along the Bangong-Nujiang suture in central Tibet (Wang et al. 2016), but its occurrence in Southeast Asia, including western Yunnan, remains cryptic.

There are four belts which may represent the Meso-Tethys or Neo-Tethys suture zone in Myanmar and western Yunnan: (1) the western ophiolite Belt roughly follows the trend of the eastern Indo-Burma Range and crops out best in the Chin Hills and Naga Hills; (2) the Tagaung-Myitkyina Belt, adjacent to the border between Myanmar and China, comprises several ophiolite complexes; (3) the Lushui-Luxi-Ruili Fault, located in western Yunnan, is the boundary between Tengchong and Baoshan terranes; (4) the Paunglaung-Mawchi Zone, located in Shan Scarps region of Myanmar, contains folded Upper Jurassic to Aptian marine sedimentary rocks (Mitchell et al. 2012). Among them, the West ophiolite Belt has been widely accepted as a southward extension of the Neo-Tethys Yarlung-Tsangpo suture (Liu et al. 2016; Searle et al. 2017), but which of the four belts represents the final closure of the Meso-Tethys ocean basin has been debated. In the Lushui-Luxi-Ruili Fault, the exposed ultramafic massifs were traditionally regarded as an important component of the Meso-Tethys Ocean, thus this

fault has been considered to represent a continuation of the Bangong-Nujiang Ocean (Xu et al. 2012; Zhu et al. 2017). According to Chu et al. (2009), however, these ultramafic peridotites are not fragments of the oceanic lithosphere, but rather are components of the ancient sub-continent lithospheric mantle; which would imply that the Lushui-Luxi-Ruili Fault does not represent a suture zone. Mitchell et al. (2012) and Ridd (2016) suggested that the Paunglaung-Mawchi Zone is the possible suture that can be traced westwards into the Bangong suture in Tibet. However, no ophiolitic rocks and radiolarian cherts have been identified in this zone and this proposal has not been universally supported (Barber et al. 2017). In contrast, typical Tethyan ophiolitic rocks crop out in the Tagaung-Myitkyina Belt and have yielded zircon U–Pb ages of 171–173 Ma from gabbro and diorite in the ophiolite (Liu et al. 2016). This age is consistent with the presence of ocean floor sediments (radiolarian cherts and Albian-Cenomanian limestones) with Late Jurassic age in the adjacent area (Mitchell et al. 2012). Importantly, the geochronology, petrology, and geochemistry of these ophiolites are essentially identical to those included in the Bangong-Nujiang suture zone within Tibet (Liu et al. 2016; Wang et al. 2016 and references therein), indicating a similar Tethys ocean basin in the Tagaung-Myitkyina Belt and the Bangong-Nujiang Ocean in Tibet. Consequently, the Meso-Tethys ocean (Bangong-Nujiang ocean) most likely extended southward into the Tagaung-Myitkyina area between the West Burma and Sibumasu terranes (Liu et al. 2016).

Based on the presence of correlated Late Carboniferous- Early Permian glacial-marine diamictites and faunas, the Tengchong terrane has been considered to be a component of the Sibumasu Terrane (Wopfner 1996; Metcalfe 2011, 2013). Alternatively, however, it has been suggested that the Tengchong terrane may be related to the Lhasa Terrane to the west (Xie et al. 2016). Nevertheless, the closely coincident dates obtained for the magmatic and tin metallogenic events in the Sibumasu and Tengchong terranes (Fig. 11) are consistent with a

close correlation between the two. Therefore, we suggest that the tin ore deposits hosted both in the Tengchong and Sibumasu terranes likely reflect the same overall tectonic history.

The timing of the Lhasa-Qiangtang collision in central Tibet remains contentious (Chen et al. 2020), but evidence from the eastern part of the Banggong-Nujiang suture zone suggests that the Meso-Tethys ocean may have closed during the Late Jurassic to Early Cretaceous (Zhu et al. 2016). In particular, Early Cretaceous magmatic rocks are widely distributed along the Bangong-Nujiang suture zone (Zhu et al. 2016; Hu et al. 2019). These rocks are interpreted to have formed in a post-collisional setting following slab break-off during the latter stages of the Lhasa-Qiangtang collision (Hu et al. 2019). Similarly, massive Early Cretaceous granitoids lying within the eastern part of the Tengchong terrane are also interpreted to have resulted from a postcollisional extensional regime following the closure of the Meso-Tethys ocean (Zhang et al. 2018). We suggest, therefore, that the Early Cretaceous (~ 125–110 Ma) Sn–W metallogenic event in the western SATB most likely formed within a post-collisional environment (Fig. 12a). As a consequence of slab break-off, upwelling of asthenosphere mantle through the slab window heated the overlying lithospheric mantle that had previously been fluxed by crustal components during previous subduction events and triggered partial melting of the enriched mantle wedge (Von Blanckenburg and Davies 1995). The mafic magmas produced by this partial melting rose into the overlying crust and induced crustal melting (Atherton and Ghani 2002; Ersoy and Palmer 2013), resulting in granitic magmatism and related Sn–W deposits (e.g., Jiaojiguan, Mawpalwa Taung; Cao et al. 2017a; Paik 2017).

By the Late Cretaceous to Paleocene (~ 90–60 Ma), the West Burma terrane had accreted to the Sibumasu-Tengchong terrane, and a new phase of Neo-Tethyan oceanic slab subduction led to the formation of the Andean-type Wuntho-Popa Arc in the West Burma terrane (Fig. 12b). Thus, the Wuntho-Popa Arc represents the southward continuation of the Gangdese Arc (Zhang et al. 2017a; Gardiner et al. 2018; Lin et al. 2019). On the basis of

integrated seismic, geochemical, and geochronology studies, Zhang et al. (2017a) suggested that the Wuntho-Popa Arc shows three discrete stages of arc magmatism during the mid-Cretaceous (110–90 Ma), latest Cretaceous–Early Paleocene (69–64.5 Ma), and Eocene (53–38 Ma) (Fig. 11c). Detrital zircon ages from the Cretaceous-Miocene successions in the Chindwin Basin (thought to represent the forearc of the Wuntho-Popa Arc) also suggest a main magmatic stage for the arc between 110 and 80 Ma, and a lesser subordinate stage between 70 and 40 Ma (Wang et al. 2014). During the long-lived magmatism (~ 110–30 Ma) in the Wuntho-Popa Arc, a magmatic lull of ~ 110–90 Ma is apparent in the WGP (Fig. 11a), and which may be related to the collision between the West Burma terrane and the Sibumasu-Tengchong terrane during the Early Cretaceous (Li et al. 2018b). Thus, we suggest that this magmatic lull was most likely caused by the fact that the subducted Neo-Tethys oceanic slab did not reach beneath the Sibumasu-Tengchong terranes until the Middle Cretaceous (Fig. 12b). After that time, widespread felsic magmatism and abundant granite-related Sn–W mineralization occurred in the western SATB since the Late Cretaceous (Fig. 11a-b).

The granitoids in the Wuntho-Popa Arc have associated copper–gold mineralization and display an affinity to I-type granites, which dominantly derive from partial melting of the mantle and/or juvenile crustal sources (Zaw 1990; Mitchell et al. 2012; Gardiner et al. 2015a, 2017; Zhang et al. 2017a). In contrast, the coeval Late Cretaceous–Paleocene S-type granites in the Sibumasu terrane are associated with Sn–W mineralization, and are mainly derived from an ancient crustal source (Jiang et al. 2017; Gardiner et al. 2018; Li et al. 2019b). The two parallel magmatic belts with different magma sources and metal mineralization characteristics in Myanmar exhibit strong similarities with the Central Andes metallogenic belt (Mlynarczyk and Williams-Jones 2005). Therefore, we proposed an Andean-type accretionary setting on the margins of the Neo-Tethys subduction in the western SATB from the Late Cretaceous to Paleocene (~90–60 Ma). During this period, subduction of the Neo-Tethyan oceanic

lithosphere led to the generation of extensive S-type felsic magmatism in the Sibumasu terrane (Fig. 12c). The felsic magmas derived from melting of the ancient Sibumasu-Tengchong crust underwent high degrees of fractional crystallization and fluid exsolution to form the abundant Sn–W deposits (e.g., Hermyingyi, Xiaolonghe; Cao et al. 2016, 2017b; Jiang et al. 2017).

India-Asia collision initially occurred at ~ 65–63 Ma within Tibet and then spread westwards and eastwards, reaching Myanmar at ~ 50 Ma (Wu et al. 2014; Ding et al. 2017; Westerweel et al. 2019). Continent–continent collision is invariably followed by oceanic slab break-off, crustal thickening, and extensive magmatism (Davies and Von Blanckenburg 1995; Atherton and Ghani 2002; Ersoy and Palmer 2013). OIB-like mafic magmatism occurred at ~42–40 Ma in the Tengchong terrane and was likely caused by the slab break-off of the subducted Neo-Tethyan oceanic slab (Xu et al. 2008). Therefore, slab break-off was likely responsible for an Early Eocene (~50–40 Ma), magmatic flare-up that occurred in the West Burma and Sibumasu-Tengchong terranes, and also led to the Sn–W mineralization event in the western SATB (Fig. 12d). Overall, the evidence from the western SATB suggests that extensive Sn mineralization is favored during both the oceanic plate subduction stage and the post-collisional stage of continent–continent collision.

Conclusions

1. Direct dating of ore minerals from nine representative primary tin ore deposits in southern Myanmar, in combination with previously published tin mineralization ages, reveals that three significant Sn metallogenic events occurred in the western Southeast Asia tin belt, during ~125–110 Ma, ~90–60 Ma, and ~50–40 Ma.

2. The three metallogenic events reflect the evolution of the geodynamic settings during continental collision. The Early Cretaceous (~125–110 Ma) Sn–W mineralization is related to post-collisional slab break-off of the Sibumasu and Tengchong terranes. The Late Cretaceous

to Paleocene (~90–60 Ma) Sn–W mineralization developed in an Andean-type accretionary setting during subduction of the Neo-Tethys oceanic lithosphere. The Early Eocene (~50–40 Ma) Sn–W mineralization may have formed in a post-collision setting after the India-Asia collision.

Acknowledgements We thank Dr. Yue-Heng Yang for assistance during wolframite U–Pb dating. The manuscript benefited from constructive reviews by Editor-in-Chief Prof. Bernd Lehmann, Associated Editor Prof. Rui-Zhong Hu, Prof. Jing-Wen Mao, Dr. Rong-Qing Zhang, and an anonymous referee.

References

Acharyya SK (2015) Indo-Burma Range: a belt of accreted microcontinents, ophiolites and Mesozoic-Paleogene flyschoid sediments. Int J Earth Sci 104:1235–1251

Arboit F, Min M, Chew D, Mitchell A, Drost K, Badenszki E, Daly JS (2021) Constraining the links between the Himalayan belt and the Central Myanmar Basins during the Cenozoic: an integrated multi-proxy detrital geochronology and trace-element geochemistry study. Geosci Front 12:657–676

Atherton MP, Ghani AA (2002) Slab breakoff: a model for Caledonian, Late Granite syn-collisional magmatism in the orthotectonic (metamorphic) zone of Scotland and Donegal, Ireland. Lithos 62:65–85

Barber A, Ridd MF, Crow M (2011) The origin, movement and assembly of the pre-Tertiary tectonic units of Thailand. In: Ridd MF, Barber A, Crow M (eds) The Geology of Thailand. The Geological Society, London, pp 507–537

Barber A, Zaw K, Crow M (2017) The pre-Cenozoic tectonic evolution of Myanmar. In: Barber A, Zaw K, Crow M (Eds.) Myanmar: Geology, Resources and Tectonics. The Geological Society, London Memoir 48: 689–714

Barley ME, Pickard AL, Zaw K, Rak P, Doyle MG (2003) Jurassic to Miocene magmatism and metamorphism in the Mogok metamorphic belt and the India-Eurasia collision in Myanmar. Tectonics 22:1019

Beckinsale RD (1979) Granite magmatism in the tin belt of Southeast Asia. In: Atherton MP, Tarney J (eds) Origin of Granite Batholiths. Shiva Publishing, Kent, pp 34–44

Belousov A, Belousova M, Zaw K, Streck MJ, Bindeman I, Meffre S, Vasconcelos P (2018) Holocene eruptions of Mt. Popa, Myanmar: volcanological evidence of the ongoing subduction of Indian Plate along Arakan Trench. J Volcano Geother Res 360:126–138

Bender F (1983) Geology of Burma. Gebriider Borntraeger, Berlin

Cao HW, Zou H, Zhang YH, Zhang ST, Zheng L, Zhang LK, Tang L, Pei QM (2016) Late Cretaceous magmatism and related metallogeny in the Tengchong area: evidence from geochronological, isotopic and geochemical data from the Xiaolonghe Sn deposit, western Yunnan, China. Ore Geol Rev 78:196–212

Cao HW, Zhang YH, Pei QM, Zhang RQ, Tang L, Lin B, Cai GJ (2017a) U-Pb dating of zircon and cassiterite from the Early Cretaceous Jiaojiguan iron-tin polymetallic deposit, implications for magmatism and metallogeny of the Tengchong area, western Yunnan, China. Inter Geol Rev 59:234–258

Cao HW, Pei QM, Zhang ST (2017b) Geology, geochemistry and genesis of the Eocene Lailishan Sn deposit in the Sanjiang region, SW China. J Asian Earth Sci 137:220–240

Charusiri P, Clark AH, Farrar E, Archibald D, Charusiri B (1993) Granite belts in Thailand: evidence from the $^{40}Ar/^{39}Ar$ geochronological and geological syntheses. J Southeast Asian Earth Sci 8:127–136

Chen XC, Hu RZ, Bi XW, Li HM, Lan JB, Zhao CH, Zhu JJ (2014) Cassiterite LA-MC-ICP-MS U/Pb and muscovite $^{40}Ar/^{39}Ar$ dating of tin deposits in the Tengchong-Lianghe tin district, NW Yunnan, China. Mineral Deposit 49:843–860

Chen XC, Hu RZ, Bi XW, Zhong H, Lan JB, Zhao CH, Zhu JJ (2015) Petrogenesis of metaluminous A-type granitoids in the Tengchong-Lianghe tin belt of southwestern China: evidences from zircon U-Pb ages and Hf–O isotopes, and wholerock Sr–Nd isotopes. Lithos 212:93–110

Chen XC, Zhao CH, Zhu JJ, Wang XS, Cui T (2018) He, Ar, and S isotopic constraints on the relationship between A-type granites and tin mineralization: a case study of tin deposits in the Tengchong-Lianghe tin belt, southwest China. Ore Geol Rev 92:316–429

Chen YF, Ding L, Li ZY, Laskowski AK, Li JX, Baral U, Qasim M, Yue YH (2020) Provenance analysis of Cretaceous peripheral foreland basin in central Tibet: implications to precise timing on the initial Lhasa-Qiangtang. Tectonophysics 775:1–17

Chu ZY, Wang W, Chen FK, Wang XL, Li XH, Ji JQ (2009) Os-Nd-Pb-Sr isotopic compositions of the Santaishan ultramafic rock in western Yunnan and its geological significances. Acta Petrol Sin 25:3221–3228 ((in Chinese with English abstract))

Cobbing EJ, Mallick DIJ, Pitfield PEJ, Teoh LH (1986) The granites of the Southeast Asian tin belt. J Geol Soc 143:537–550

Cobbing EJ, Pitfield P, Darbyshire D, Mallick D (1992) The granites of the Southeast Asian tin belt. Overseas Memoirs of the British Geological Survey. Overseas Memoir 10:369

Crow M, Zaw K (2017) Geochronology in Myanmar. In: Barber A, Zaw K, Crow M (eds) Myanmar: geology, resources and tectonics. The Geological Society, London Memoir 48:713–759

Davies JH, von Blanckenburg F (1995) Slab breakoff: a model of lithosphere detachment and its test in the magmatism and deformation of collisional orogens. Earth Planet Sci Lett 129:85 102

Deng XD, Luo T, Li JW, Hu ZC (2019) Direct dating of hydrothermal tungsten mineralization using in situ wolframite U-Pb chronology by laser ablation ICP-MS. Chem Geol 515:94–104

Dew REC, Collins AS, Glorie S, Morley CK, Blades ML, Nachtergaele S, King R, Foden J, De Grave J, Kanjanapayont P, Evans NJ, Alessio BL, Charusiri P (2018) Probing into Thailand's basement: new insights from U-Pb geochronology, Sr Sm–Nd, Pb and Lu–Hf isotopic systems from granitoids. Lithos 320–321:332–354

Ding L, Maksatbek S, Cai FL, Wang HQ, Song PP, Ji WQ, Xu Q, Zhang LY, Muhammad Q, Upendra B (2017) Processes of initial collision and suturing between India and Asia. Sci China-Earth Sci 60(4):635–651

Ersoy EY, Palmer MR (2013) Eocene-Quaternary magmatic activity in the Aegean: implications for mantle metasomatism and magma genesis in an evolving orogeny. Lithos 180-181:5–24

Gardiner NJ, Searle MP, Robb LJ, Morley CK (2015a) Neo-Tethyan magmatism and metallogeny in Myanmar-an Andean analogue? J Asian Earth Sci 106:197–215

Gardiner NJ, Sykes JP, Trench A, Robb LJ (2015b) Tin mining in Myanmar: production and potential. Resour Policy 46:219–233

Gardiner NJ, Robb LJ, Morley CK, Searle MP, Cawood PA, Whitehouse MJ, Kirkland CL, Roberts NMW, Myint TA (2016a) The tectonic and metallogenic framework of Myanmar: a Tethyan mineral system. Ore Geol Rev 79:26–45

Gardiner NJ, Searle MP, Morley CK, Whitehouse MP, Spencer CJ, Robb LJ (2016b) The closure of Paleo-Tethys in eastern Myanmar and northern Thailand: new insights from zircon U-Pb and Hf isotope data. Gondwana Res 39:401–422

Gardiner NJ, Hawkesworth CJ, Robb LJ, Whitehouse MJ, Roberts NM, Kirkland CL, Evans NJ (2017) Contrasting granite metallogeny through the Zircon record: a case study from Myanmar. Sci Rep
7:748

Gardiner NJ, Searle MP, Morley CK, Robb LJ, Whitehouse MJ, Roberts NMW, Kirkland CL, Spencer CJ (2018) The crustal architecture of Myanmar imaged through zircon U-Pb, Lu–Hf and O isotopes: tectonic and metallogenic implications. Gondwana Res 62:27–60

Griffin WL, Powell W, Pearson NJ, Reilly SYO' (2008) GLITTER: data reduction software for laser ablation ICP-MS. Mineral Assoc Can Short Course 40:308–311

Gulson BL, Jones MT (1992) Cassiterite: potential for direct dating of mineral deposits and a precise age for the Bushveld Complex granites. Geology 20:355–358

Hall R (2012) Late Jurassic-Cenozoic reconstructions of the Indonesian region and the Indian Ocean. Tectonophysics 570–571:1–41

Heinrich CA (1990) The chemistry of tin (-tungsten) ore deposition. Econ Geol 85:457–481

Hou ZQ, Zhang HR (2015) Geodynamics and metallogeny of the eastern Tethyan metallogenic domain. Ore Geol Rev 70:346–348

Hou ZQ, Zaw K, Pan GT, Mo XX, Xu Q, Hu YZ, Li XZ (2007) Sanjiang Tethyan metallogenesis in S.W. China: tectonic setting, metallogenic epochs and deposit types. Ore Geol Rev 31:48–87

Htun T, Htay T, Zaw K (2017) Tin-tungsten deposits of Myanmar. Geol Soc London Memoirs 48:625–647

Htun TK, Yonezu K, Myint AZ, Tindell T, Watanabe K (2019) Petrogenesis, ore mineralogy, and fluid inclusion studies of the Tagu Sn–W deposit, Myeik, Southern Myanmar. Minerals 9:654

Hu WL, Wang Q, Yang JH, Zhang C, Tang GJ, Ma L, Qi Y, Yang ZY, Sun P (2019) Late early Cretaceous peraluminous biotite granites along the Bangong-Nujiang suture zone, Central Tibet: products derived by partial melting of metasedimentary rocks? Lithos 344–345:147–158

Hutchison CS (1993) Gondwana and Cathaysian blocks, Palaeotethys sutures and Cenozoic tectonics in South-east Asia. Geol Rundsch 82:388–405

Hutchison CS, Taylor D (1978) Metallogenesis in SE Asia. J Geol Soc 135:407–428

Jiang H, Jiang SY, Li WQ, Zhao KD (2019) Timing and source of the Hermyingyi W-Sn deposit in southern Myanmar, SE Asia: evidence from molybdenite Re–Os age and sulfur isotopic composition. J Earth Sci 30:70–79

Jiang H, Li WQ, Jiang SY, Wang H, Wei XP (2017) Geochronological, geochemical and Sr–Nd–Hf isotopic constraints on the petrogenesis of Late Cretaceous A-type granites from the Sibumasu Block, Southern Myanmar, SE Asia. Lithos 268–271:32–47

Lee HY, Chung SL, Yang HM (2016) Late Cenozoic volcanism in central Myanmar: geochemical characteristics and geodynamic significance. Lithos 245:174–190

Lehmann B (1990) Metallogeny of tin. Springer, Berlin

Lehmann B (2020) Formation of tin ore deposits: a reassessment. Lithos. https:// doi. org/ 10. 1016/j. lithos. 2020. 105756

Lehmann B, Jungyusuk N, Khositanont S, Hohndorf A, Kuroda Y (1994) The tin-tungsten ore system of Pilok, Thailand. J Southeast Asian Earth Sci 10:51–63

Li RY, Mei LF, Zhu GH, Zhao RM, Xu XM, Zhao HX, Zhang P, Yin YP, Ma YX (2013) Late mesozoic to cenozoic tectonic events in volcanic arc, West Burma Block: evidences from U-Pb zircon dating and apatite fission track data of granitoids. J Earth Sci 24:553–568

Li CY, Zhang RQ, Ding X, Ling MX, Fan WM, Sun WD (2016) Dating cassiterite using laser ablation ICP-MS. Ore Geol Rev 72:313–322

Li H, Myint AZ, Yonezu K, Watanabe K, Algeo TJ, Wu JH (2018a) Geochemistry and U-Pb geochronology of the Wagone and Hermyingyi A-type granites, southern Myanmar: implications for tectonic setting, magma evolution and Sn–W mineralization. Ore Geol Rev 95:575–592

Li JX, Zhang LY, Fan WM, Ding L, Sun YL, Peng TP, Li GM, Sein K (2018b) Mesozoic-Cenozoic tectonic evolution and metallogeny in Myanmar: evidence from zircon/cassiterite U-Pb and molybdenite Re–Os geochronology. Ore Geol Rev 102:829–845

Li JX, Fan WM, Zhang LY, Ding L, Sun YL, Peng TP, Cai FL, Guan QY, Sein K (2019a) Subduction of Indian continental lithosphere constrained by Eocene-Oligocene magmatism in northern Myanmar. Lithos 348–349:105211

Li JX, Fan WM, Zhang LY, Evans NJ, Sun YL, Ding L, Guan QY, Peng TP, Cai FL, Sein K (2019b) Geochronology, geochemistry and Sr–Nd–Hf isotopic compositions of Late

Cretaceous-Eocene granites in southern Myanmar: petrogenetic, tectonic and metallogenic implications. Ore Geol Rev 112:1–16

Li JX, Fan WM, Zhang LY, Ding L, Yue YH, Xie J, Cai FL, Quan QY, Sein K (2020a) Biotite geochemistry deciphers magma evolution of Sn-bearing granite, southern Myanmar. Ore Geol Rev 121:1–13

Li JX, Fan WM, Zhang LY, Peng TP, Sun YL, Ding L, Yue YH, Xie J, Cai FL, Quan QY, Sein K (2020b) Prolonged Neo-Tethyan magmatic arc in Myanmar: evidence from geochemistry and Sr–Nd–Hf isotopes of Cretaceous mafic–felsic intrusions in the Banmauk-Kawlin area. Inter J Earth Sci 109:1–20

Licht A, Win Z, Westerweel J, Nathan C, Morley CK, Chantraprasert S, Poblete F, Ugrai T, Nelson B, Auang DW, Dupont-Nivet G (2020) Magmatic history of central Myanmar and implications for the evolution of the Burma terrane. Gondwana Res 87:303–319

Lin TH, Mitchell AHG, Chung SL, Tan XB, Tang JT, Oo T, Wu FY (2019) Two parallel magmatic belts with contrasting isotopic characteristics from southern Tibet to Myanmar: zircon U-Pb and Hf isotopic constraints. J Geol Soc 176:574–587

Liu CZ, Chung SL, Wu FY, Zhang C, Xu Y, Wang JG, Chen Y, Guo S (2016) Tethyan suturing in Southeast Asia: zircon U-Pb and Hf-O isotopic constraints from Myanmar ophiolites. Geology 44:311–314

Liu YS, Gao S, Hu ZC, Gao CG, Zong KQ, Wang DB (2010) Continental and oceanic crust recycling-induced melt-peridotite interactions in the Trans-North China Orogen: U-Pb dating, Hf isotopes and trace elements in zircons from mantle xenoliths. J Petrol 51:537–571

Ludwig KR (2012) Isoplot: a geochronological toolkit for Microsoft Excel. Berkeley Geochronology Certer Special Publication No. 5, pp 1–75

Luo T, Deng XD, Li JW, Hu ZC, Zhang W, Liu YS, Zhang JF (2019) U-Pb geochronology of wolframite by laser ablation inductively coupled plasma mass spectrometry. J Anal at Spectrom 34:1439–1446

Ma N, Deng J, Wang QF, Wang CM, Zhang J, Li GJ (2013) Geochronology of the Dasongpo tin deposit, Yunnan Province: evidence from zircon LA-ICP-MS U-Pb ages and cassiterite LA-MC-ICPMS U–Pb age. Acta Petrol Sin 29:1223–1235 (in Chinese with English Abstract)

Mao JW, Ouyang H, Song S, Santosh M, Yuan S, Zhou Z, Zheng W, Liu H, Liu P, Cheng Y, Chen M (2019) Geology and metallogeny of tungsten and tin deposits in China. Soc Econ Geol Spec Publ 22:411–482

Mao W, Zhong H, Yang JH, Tang YW, Liu L, Fu YZ, Zhang XC, Sein K, Aung SM, Li J, Zhang L (2020) Combined zircon, molybdenite, and cassiterite geochronology and cassiterite geochemistry of the Kuntabin Tin-Tungsten Deposit in Myanmar. Econ Geol 115:603–625

Maury RC, Pubellier M, Rangin C, Wulput L, Cotten J, Socquet A, Bellon H, Guillaud JP, Htun HM (2004) Quaternary calc-alkaline and alkaline volcanism in an hyper-oblique convergence setting, central Myanmar and western Yunnan. Bulletin De La Societe Geologique De France 175:461–472

Metcalfe I (2011) Palaeozoic-Mesozoic history of SE Asia. Geol Soc Lond Spec Publ 355:7 35

Metcalfe I (2013) Gondwana dispersion and Asian accretion: tectonic and palaeogeographic evolution of eastern Tethys. J Asian Earth Sci 66:1–33

Mitchell AHG (1977) Tectonic settings for the emplacement of Southeast Asian tin granites. Geol Soc Malaysia 9:123–140

Mitchell AHG (1979) Rift-, subduction- and collision-related tin belts. Geol Soc Malaysia 11:81–102

Mitchell AHG (1986) Mesozoic and Cenozoic regional tectonics and metallogenesis in Mainland SE Asia. Geol Soc Malaysia, Bulletin 20:221–239

Mitchell AHG (2018) Geological belts, plate boundaries, and mineral deposits in Myanmar. Elsevier

Mithchell AHG, Garson MS (1981) Mineral deposit and global tectonic settings. Academic Press, London

Mitchell A, Chung SL, Oo T, Lin TH, Hung CH (2012) Zircon U-Pb ages in Myanmar: magmatic-metamorphic events and the closure of a Neo-Tethys ocean? J Asian Earth Sci 56:1-23

Mlynarczyk MS, Williams-Jones AE (2005) The role of collisional tectonics in the metallogeny of the Central Andean tin belt. Earth Planet Sci Lett 240:656–667

Morley CK, Searle M (2017) Regional tectonics, structure and evolution of the Andaman-Nicobar Islands from ophiolite formation and obduction to collision and back-arc spreading. Geol Soc Lond Memoirs 47:51–74

Moscati RJ, Neymark LA (2020) U-Pb geochronology of tin deposits associated with the Cornubian Batholith of southwest England: direct dating of cassiterite by in situ LA-ICPMS. Mineral Deposita 55:1–20

Myint AZ, Zaw K, Swe YM, Yonezu K, Cai Y, Manaka T, Watanabe K (2017) Geochemistry and geochronology of granites hosting the Mawchi Sn–W deposit, Myanmar: implications for tectonic setting and emplacement. Geol Soc Lond Memoirs 48:385–400

Myint AZ, Yonezu K, Boyce AJ, Selby D, Schersten A, Tindell T, Watanabe K, Swe YM (2018) Stable isotope and geochronological study of the Mawchi Sn–W deposit, Myanmar: implications for timing of mineralization and ore genesis. Ore Geol Rev 95:663–679

Neymark LA, Holm-Denoma CS, Moscati RJ (2018) In situ LA-ICPMS U-Pb dating of cassiterite without a known-age matrix-matched reference material: examples from worldwide tin deposits spanning the Proterozoic to the Tertiary. Chem Geol 483:410–425

Ng SWP, Chung SL, Robb LJ, Searle MP, Ghani AA, Whitehouse MJ, Oliver GJH, Sone M, Gardiner NJ, Roselee MH (2015a) Petrogenesis of Malaysian granitoids in the Southeast Asian tin belt: Part 1. Geochemical and Sr–Nd isotopic characteristics. Geol Soc Am Bull 127:1209–1237

Ng SWP, Whitehouse MJ, Searle MP, Robb LJ, Ghani AA, Chung SL, Oliver GJH, Sone M, Gardiner NJ, Roselee MH (2015b) Petrogenesis of Malaysian granitoids in the Southeast Asian tin belt: Part 2. U-Pb zircon geochronology and tectonic model. Geol Soc Am Bull 127:1238–1258

Paik M (2017) Geochemistry and geochronology of granitoid rocks in the Mawpalaw Taung area, Thanbyuzayat Township, southern Myanmar: their petrogenesis and tectonic setting. Geol Soc Lond Memoirs 48:401–412

Paton C, Hellstrom J, Paul B, Woodhead J, Hergt J (2011) Iolite: freeware for the visualization and processing of mass spectrometric data. J Anal at Spectrom 26:2508–2518

Pickard AL, Barley ME, Zaw K (1996) Zircon SHRIMP ages for a selection of granites from Myanmar. In: South East Asia Granite Geochronology Report, Key Centre for Strategic Mineral Deposits, Department of Geology and Geophysics, University of Western Australia, Nedlands, pp 1–35

Ridd MF (2016) Should Sibumasu be renamed Sibuma? The case for a discrete Gondwana-derived block embracing western Myanmar, upper Peninsular Thailand and NE Sumatra. J Geol Soc 173:249–264

Ridd MF (2017) The Karen-Tenasserim unit. In: Barber A, Zaw K, Crow M (eds) Myanmar: geology, resources and tectonics. The Geological Society, London Memoir 48:365–384

Romer LF, Luders V (2006) Direct dating of hydrothermal W mineralization: U-Pb age for hubnerite ($MnWO_4$), Sweet Home Mine, Colorado. Geochim Cosmochim Acta 70:4725–4733

Romer RL, Kroner U (2016) Phanerozoic tin and tungsten mineralization-tectonic controls on the distribution of enriched protoliths and heat sources for crustal melting. Gondwana Res 31:60–95

Schwartz MO, Rajah SS, Askury AK, Putthapiban P, Djaswadi S (1995) The Southeast Asian tin belt. Earth Science Review 38:95–293

Searle MP, Whitehouse MJ, Robb L, Ghani AA (2012) Tectonic evolution of the Sibumasu-Indochina terrane collision zone in Thailand and Malaysia: constraints from new U-Pb zircon chronology of SE Asian tin granitoids. J Geol Soc 169:489–500

Searle MP, Morley CK, Waters DJ, Gardiner NJ, Htun KU, Nu TT, Robb LJ (2017) Tectonic and metamorphic evolution of the Mogok Metamorphic and Jade Mines belts and ophiolitic terranes of Burma (Myanmar). In: Barber A, Khin Z, Crow M (Eds.) Myanmar: geology, resources and tectonics, 48 ed. The Geological Society, London Memoir 48: 261–293

Searle MP, Noble SR, Cottle JM, Waters DJ, Mitchell AHG, Tin H, Horstwood MSA (2007) Tectonic evolution of the Mogok metamorphic belt, Burma (Myanmar) constrained by U-Th-Pb dating of metamorphic and magmatic rocks. Tectonics 26. https:// doi.org/ 10. 1029/ 2006tc0020 83

Sone M, Metcalfe I (2008) Parallel Tethyan sutures in mainland Southeast Asia: new insights for Palaeo-Tethys closure and implications for the Indosinian orogeny. CR Geosci 340:166–179

Stacey JS, Kramers JD (1975) Approximation of terrestrial lead isotope evolution by a two-stage model. Earth Planet Sci Lett 26:207–221

Tera F, Wasserburg GJ (1972) U-Th–Pb systematics in three Apollo 14 basalts and the problem of initial Pb in lunar rocks. Earth Planet Sci Lett 14:281–304

UNDGSE (1979) Mineral exploration in selected areas, Burma. Technical Report No. 6. United Nations Development Programme, DP/UN/BUR-72–002/15. United Nations, New York.

Von Blanckenburg F, Davies JH (1995) Slab breakoff: a model for syncollisional magmatism and tectonics in the Alps. Tectonics 14:120–131

Wang JG, Wu FY, Tan XC, Liu CZ (2014) Magmatic evolution of the Western Myanmar Arc documented by U-Pb and Hf isotopes in detrital zircon. Tectonophysics 612–613:97–105

Wang BD, Wang LQ, Chung SL, Chen JL, Yin FG, Liu H, Li XB, Chen LK (2016) Evolution of the Bangong-Nujiang Tethyan ocean: insights from the geochronology and geochemistry of mafic rocks within ophiolites. Lithos 245:18–33

Westerweel J, Roperch P, Licht A, Dupont-Nivet G, Win Z, Poblete F, Ruffet G, Swe HH, Thi MK, Aung DW (2019) Burma Terrane part of the Trans-Tethyan arc during collision with India according to palaeomagnetic data. Nat Geosci 12:863–868

Wopfner H (1996) Gandwana origin of the Baoshan and Tengchong terranes of west Yunnan. Geol Soc Lond Spec Publ 106:539–547

Wu FY, Ji WQ, Wang JG, Liu CZ, Chung SL, Clift PD (2014) Zircon U-Pb and Hf isotopic constraints on the onset time of India-Asia collision. Am J Sci 314:548–579

Wu HY, Deng J, Wang QF, Zhang LC, Cui XL, Shu QH, Zhang QW, Zhou SM (2019) SIMS U-Pb zircon geochronological and geochemical study of the Sn deposits in Tengchong, north of the Southeast Asian metallogenic belt: implications for the timing of mineralization and ore genesis. Ore Geol Rev 111:1–21

Xie JC, Zhu DC, Dong G, Zhao ZD, Wang Q, Mo X (2016) Linking the Tengchong Terrane in SW Yunnan with the Lhasa Terrane in southern Tibet through magmatic correlation. Gondwana Res 39:217–229

Xu YG, Lan JB, Yang QJ, Huang XL, Qiu HN (2008) Eocene break–off of the Neo-Tethyan slab as inferred from intraplate–type mafic dykes in the Gaoligong orogenic belt, eastern Tibet. Chem Geol 255:439–453

Xu YG, Yang QJ, Lan JB, Luo ZY, Huang XL, Shi YR, Xie LW (2012) Temporal-spatial distribution and tectonic implications of the batholiths in the GaoligongTengliang-Yingjiang area, western Yunnan: constraints from zircon U-Pb ages and Hf isotopes. J Asian Earth Sci 53:151–175

Yang HM (2008) Late Cenozoic volcanic rocks from Burma: geochemical characteristics and petrogenesis. M. Sc. Thesis, National Taiwan University

Yang M, Yang YH, Wu ST, Romer RL, Che XD, Zhao ZF, Li WS, Yang JH, Wu FY, Xie LW, Huang C, Zhang D, Zhang Y (2020) Accurate and precise in situ U-Pb isotope dating of wolframite series minerals via LA-SF-ICP-MS. J Anal at Spectrom 35:2191–2203

Yuan SD, Peng JT, Hao S, Li HM, Geng JZ, Zhang DL (2011) In situ LA-MC-ICPMS and ID-TIMS U-Pb geochronology of cassiterite in the giant Furong tin deposit, Hunan Province, South China: new constraints on the timing of tin-polymetallic mineralization. Ore Geol Rev 43:235–242

Yuan SD, Peng JT, Hu RZ, Li HM, Shen NP, Zhang DL (2008) A precise U-Pb age on cassiterite from the Xianghualing tinpolymetallic deposit (Hunan, South China). Mineral Deposit 43:375–382

Zaw K (1984) Geology and geothermometry of vein-type W-Sn deposits at Pennaichaung and Yetkanzintaung prospects, Tavoy Township, Tennasserim Division, southern Myanmar. Mineral Deposit 19:138–144

Zaw K (1990) Geological, petrological and geochemical characteristics of granitoid rocks in Myanmar: with special reference to the associated W-Sn mineralization and their tectonic setting. J SE Asian Earth Sci 4:293–335

Zaw K, Meffre S, Lai CK, Burrett C, Santosh M, Graham I, Manaka T, Salam A, Kamvong T, Cromie P (2014) Tectonics and metallogen of mainland Southeast Asia-a review and contribution. Gondwana Res 26:5–30

Zhang P, Mei LF, Hu XL, Li RY, Wu LL, Zhou ZC, Qiu HN (2017a) Structures, uplift, and magmatism of the Western Myanmar Arc: constraints to mid-Cretaceous-Paleogene tectonic evolution of the western Myanmar continental margin. Gondwana Res 52:18–38

Zhang RQ, Lehmann B, Seltmann R, Sun WD, Li CY (2017b) Cassiterite U-Pb geochronology constrains magmatic-hydrothermal evolution in complex evolved granite systems: the classic Erzgebirge tin province (Saxony and Bohemia). Geology 45:1095–1098

Zhang JY, Peng TP, Fan WM, Zhao GC, Dong XH, Gao JF, Peng BX, Wei C, Xia XP, Chen LL, Liang XR (2018) Petrogenesis of the Early Cretaceous granitoids and its mafic enclaves in the Northern Tengchong Terrane, southern margin of the Tibetan Plateau and its tectonic implications. Lithos 318–319:283–298

Zhou XP, Qi HW, Qu WJ, Li C (2017) Re–Os isotopic dating for molybdenites in Xinqi Tungsten-Tin polymetallic deposit of Yunnan province, China and its geological significance. Acta Mineralogica Sinica 37:84–92 (in Chinese with English abstract)

Zhu DC, Li SM, Cawood PA, Wang Q, Zhao ZD, Liu SA, Wang LQ (2016) Assembly of the Lhasa and Qiangtang terranes in central Tibet by divergent double subduction. Lithos 245:7–17

Zhu RZ, Lai SC, Santosh M, Qin JF, Zhao SW (2017) Early Cretaceous Na-rich granitoids and their enclaves in the Tengchong Block, SW China: magmatism in relation to subduction of the Bangong-Nujiang Tethys ocean. Lithos 286:175–190

Figure Captions

Figure 1. a Regional geological map showing the principal continental terranes, sutures, and granitoid provinces of Southeast Asia (modified after Searle et al. 2012; Gardiner et al. 2016a). **b** A schematic map showing the tectonic framework, spatial–temporal distribution of magmatic rocks and main tin deposits in Myanmar and its adjacent area (modified after Sone and Metcalfe 2008; Li et al. 2018a; Myint et al. 2018).

Figure 2. Simplified geological map of the Hermyingyi Sn–W deposit (modified after Jiang et al. 2019).

Figure 3. Representative photographs of quartz veins from typical Sn–W deposits. **a**–**b** Wolframite-cassiterite-sulfide-quartz veins from the Hermyingyi deposit. **C** Wolframite-cassiterite-quartz veins from the Thaling Taung deposit. **D** Wolframite-cassiterite-sulfide-quartz veins from the Letha Taung deposit.

Figure 4. a–**r** Photographs and photomicrographs (cross-polarized light) of cassiterite ores from nine Sn–W deposits in southern Myanmar. Abbreviations: Cst = cassiterite, Wlf = wolframite, Qtz = quartz, Py = pyrite, Mus = muscovite.

Figure 5. a–**r** Photographs and photomicrographs (reflected light) of wolframite ores from nine Sn–W deposits in southern Myanmar. Abbreviations are as defined in the Fig. 4 caption.

Figure 6. Representative scanning electron microscope (SEM) cathodoluminescence (CL) images of cassiterite grains used for U–Pb dating. **a**–**i** cassiterite grains from the Hermyingyi, Thitkhatoe, Thaling Taung, Kalonta, Taungphila, Pagaye, Bawapin, Kanbauk, and Letha Taung deposits, respectively. The spot size of the laser beam is 50 μm (white circles).

Figure 7. Tera-Wasserburg (T-W) Concordia diagrams and ^{207}Pb-corrected weighted mean ^{206}Pb/^{238}U ages of cassiterite samples from the nine Sn–W deposits in southern Myanmar.

Figure 8. Tera-Wasserburg (T-W) Concordia diagrams and 207Pb-corrected weighted mean ^{206}Pb/^{238}U ages of wolframite samples from the nine Sn–W deposits in southern Myanmar.

Figure 9. Compilation of geochronological data for the the nine Sn–W deposits in southern Myanmar. The data sources are shown in Table 2.

Figure 10. Spatial–temporal distribution of Mesozoic-Cenozoic tin deposits in the western SATB. Data of Sn deposits are from Lehmann et al. (1994), Ma et al. (2013), Chen et al. (2014), Cao et al. (2016, 2017a), Gardiner et al. (2016a), Myint et al. 2017, 2018), Paik (2017), Zhou et al. (2017), Li et al. (2018b, 2019b), Jiang et al. (2019), Wu et al., (2019), Mao et al. (2020) and this study.

Figure 11. a Igneous rock ages (zircon U–Pb ages) from the WGP. **B** Sn–W mineralization ages (cassiterite U–Pb ages, zircon U–Pb ages, wolframite U–Pb ages, molybdenite Re–Os ages, muscovite Ar–Ar ages, including data from this study) from the western SATB. **c** Igneous rock ages (Ar–Ar and K–Ar ages, zircon U–Pb ages) from the Wuntho-Popa Arc. Data of the WGP are from Barley et al. (2003), Searle et al. (2007), Mitchell et al. (2012), Gardiner et al. (2016a, 2017, 2018), Xie et al. (2016), Crow and Zaw (2017), Jiang et al. (2017), Myint et al. (2017), Paik (2017), Dew et al. (2018), Li et al. (2018b, 2019a), Lin et al. (2019), Mao et al. (2020), and references therein. Data of the western SATB are from Lehmann et al. (1994), Ma et al. (2013), Chen et al. (2014), Cao et al. (2016, 2017a), Gardiner et al. (2016a), Myint et al., 2017, 2018), Paik (2017), Zhou et al. (2017), Li et al. (2018b, 2019b), Jiang et al. (2019), Wu et al. (2019), Mao et al. (2020) and this study. Data of the Wuntho-Popa Arc are from Barley et al. (2003), Gardiner et al. (2016a, 2017), Zhang et al. (2017a), Li et al. (2013), Mitchell et al. (2012), Lin et al. (2019), Li et al. (2019a, 2020b), Belousov et al. (2018), Licht et al. (2020), Arboit et al. (2021), UNDGSE. (1979), Yang (2008), Lee et al. (2016), Maury et al. (2004), and Westerweel et al. (2019).

Figure 12. a–**d** Schematic models for Late Cretaceous–Eocene (125–40 Ma) granites and associated Sn–W mineralization in the western Southeast Asia tin belt.

Figure 1

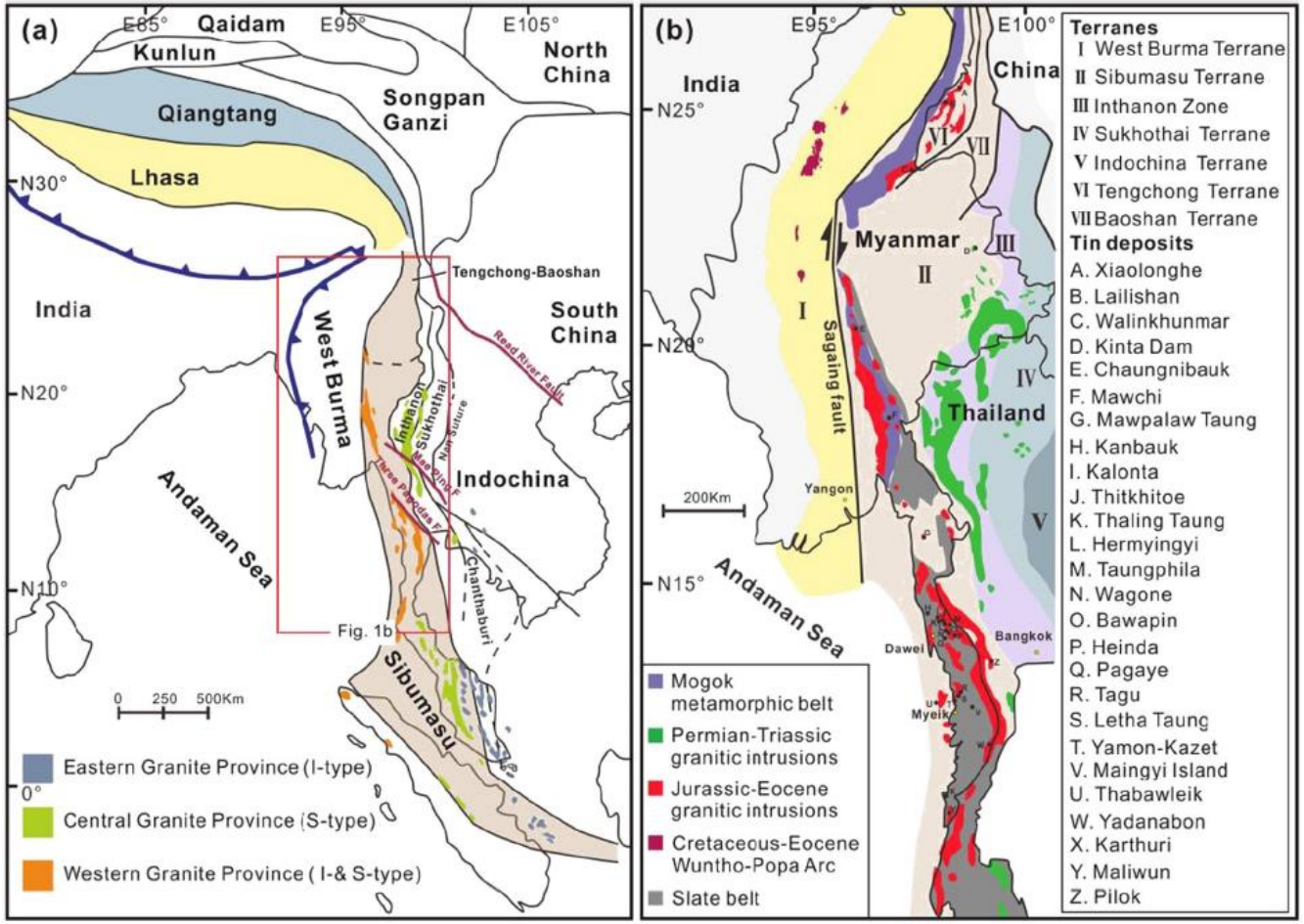
(a)
E85°
Qaidam
Kunlun
E95°
E105°
North China
Songpan Ganzi
Qiangtang
Lhasa
N30°
India
Tengchong-Baoshan
South China
West Burma
Red River Fault
N20°
Inthanon
Sukhothai
Nan suture
Mae Ping F.
Three Pagodas F.
Indochina
Andaman Sea
Chanthaburi
N10°
Fig. 1b
Sibumasu
0
250
500Km
0°
Eastern Granite Province (I-type)
Central Granite Province (S-type)
Western Granite Province (I-& S-type)
(b)
E95°
E100°
India
China
N25°
VI
VII
Myanmar
III
II
I
Sagaing fault
N20°
IV
Thailand
200Km
Yangon
V
N15°
Andaman Sea
Dawei
Bangkok
Myeik
Mogok metamorphic belt
Permian-Triassic granitic intrusions
Jurassic-Eocene granitic intrusions
Cretaceous-Eocene Wuntho-Popa Arc
Slate belt
Terranes
I West Burma Terrane
II Sibumasu Terrane
III Inthanon Zone
IV Sukhothai Terrane
V Indochina Terrane
VI Tengchong Terrane
VII Baoshan Terrane
Tin deposits
A. Xiaolonghe
B. Lailishan
C. Walinkhunmar
D. Kinta Dam
E. Chaungnibauk
F. Mawchi
G. Mawpalaw Taung
H. Kanbauk
I. Kalonta
J. Thitkhitoe
K. Thaling Taung
L. Hermyingyi
M. Taungphila
N. Wagone
O. Bawapin
P. Heinda
Q. Pagaye
R. Tagu
S. Letha Taung
T. Yamon-Kazet
V. Maingyi Island
U. Thabawleik
W. Yadanabon
X. Karthuri
Y. Maliwun
Z. Pilok

Figure 2

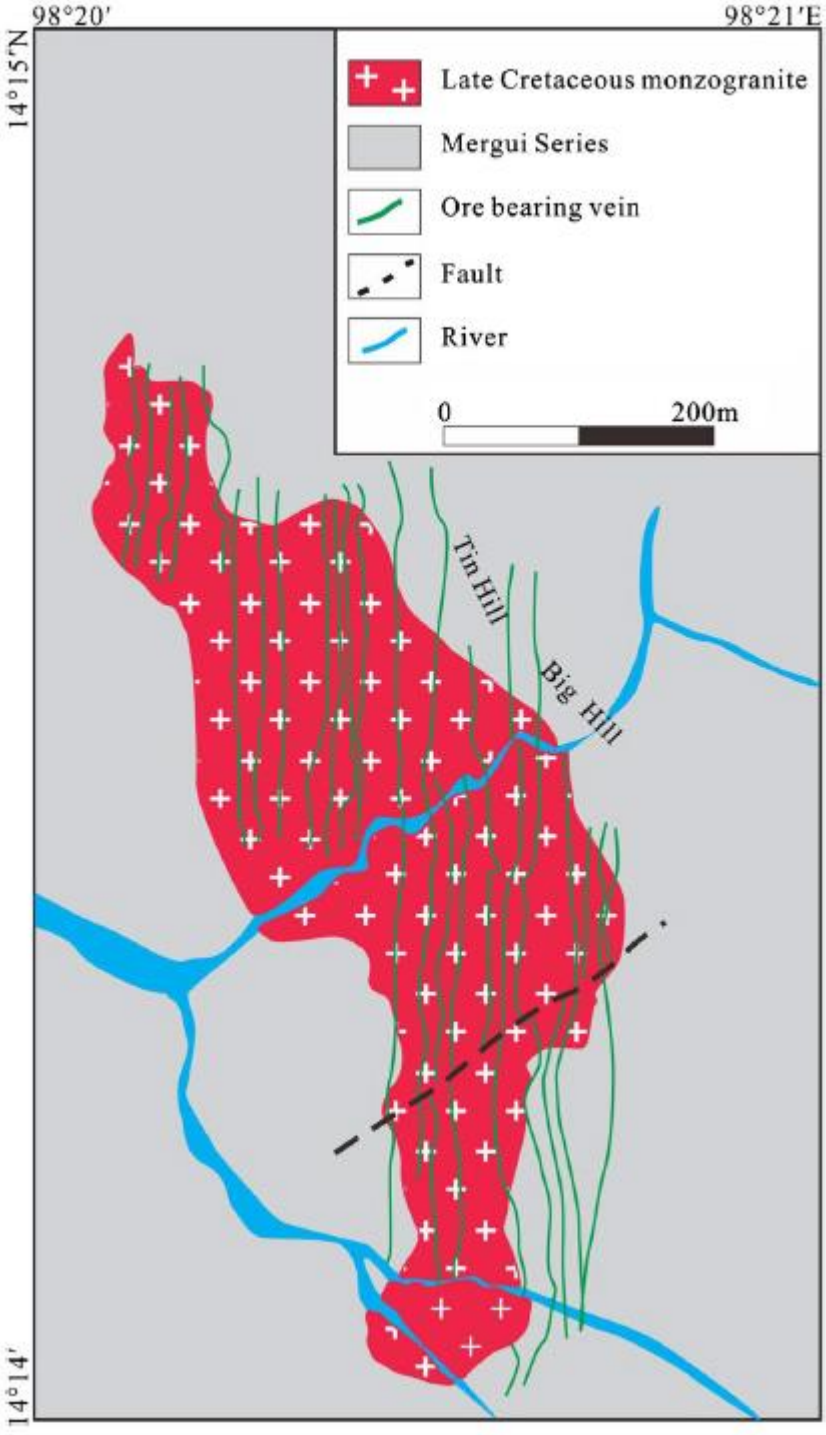
98°20′
98°21′E
14°15′N
14°14′
Late Cretaceous monzogranite
Mergui Series
Ore bearing vein
Fault
River
0
200m
Tin Hill
Big Hill

Figure 3.

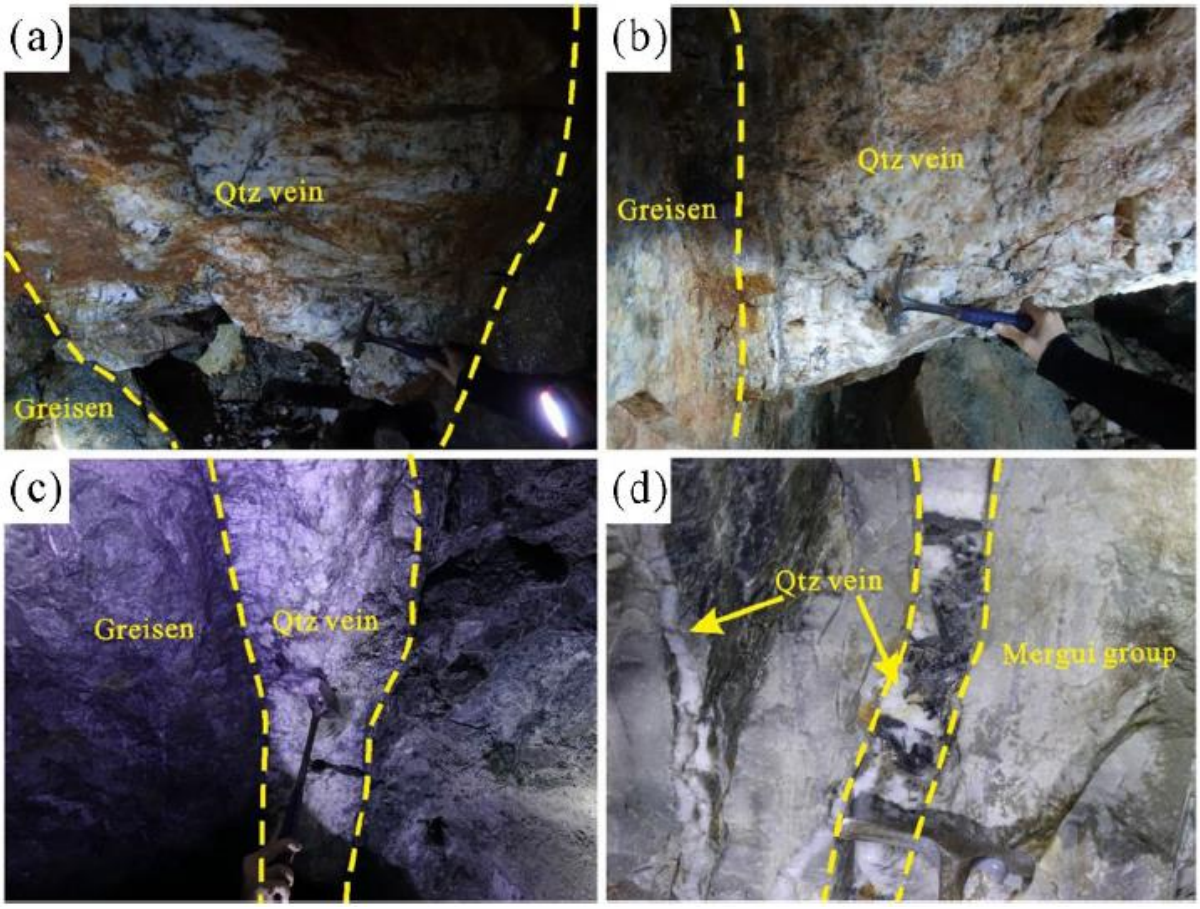
(a)
Qtz vein
Greisen
(b)
Qtz vein
Greisen
(c)
Greisen
Qtz vein
(d)
Qtz vein
Mergui group

Figure 4.

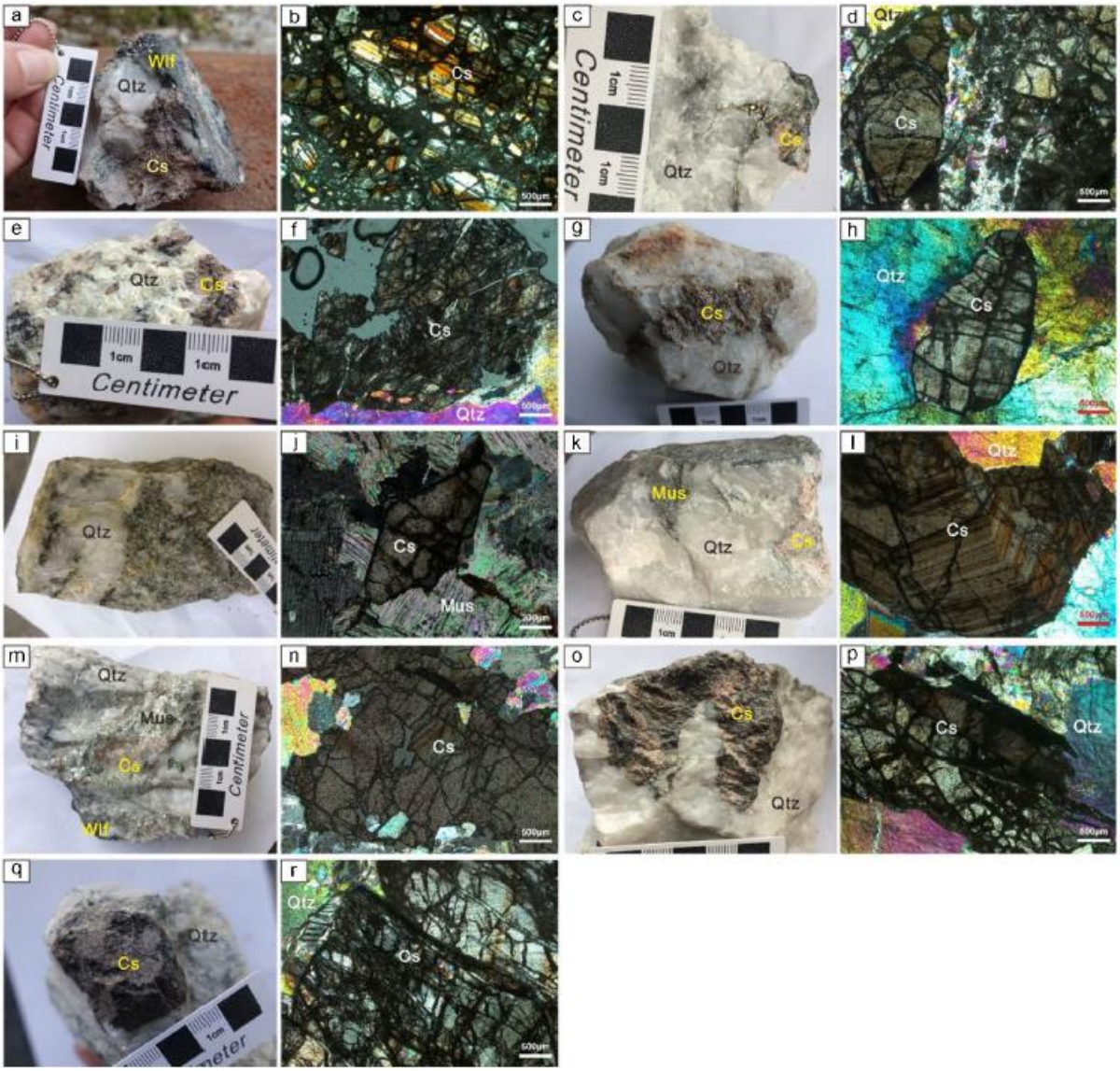
a
Wlf
Qtz
Cs
Centimeter
b
Cs
c
Centimeter
1cm
1cm
Py
Cs
Qtz
d
Qtz
Cs
e
Qtz
Cs
1cm
1cm
Centimeter
f
Cs
Qtz
g
Cs
Qtz
h
Qtz
Cs
i
Qtz
j
Cs
Mus
k
Mus
Qtz
Cs
l
Qtz
Cs
m
Qtz
Mus
Cs
Wlf
Centimeter
n
Cs
o
Cs
Qtz
p
Cs
Qtz
q
Qtz
Cs
r
Qtz
Cs

Figure 5.

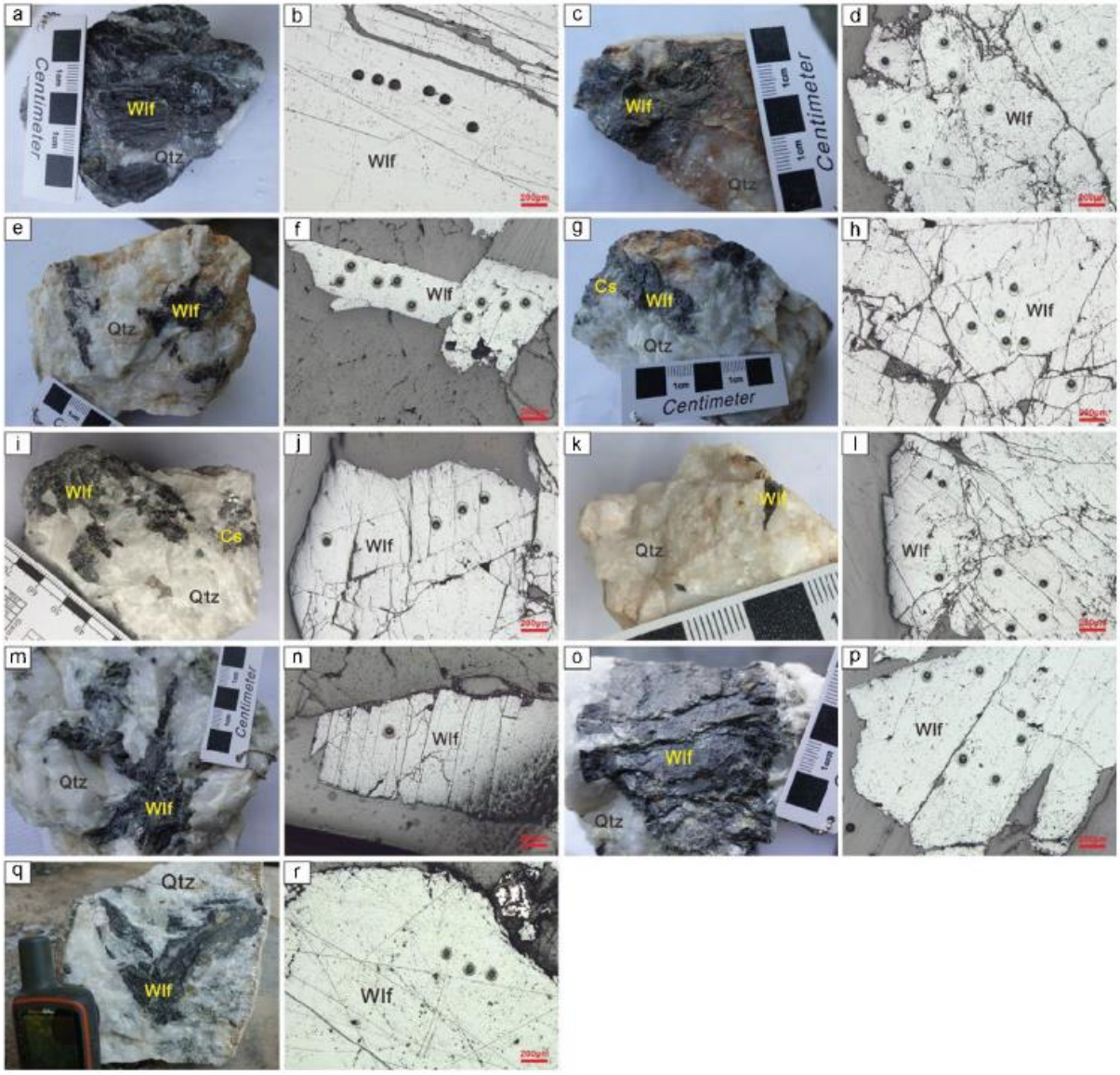
a
Centimeter
Wlf
Qtz
b
Wlf
c
Wlf
Qtz
Centimeter
d
Wlf
e
Qtz
Wlf
f
Wlf
g
Cs
Wlf
Qtz
Centimeter
h
Wlf
i
Wlf
Cs
Qtz
j
Wlf
k
Wlf
Qtz
l
Wlf
m
Centimeter
Qtz
Wlf
n
Wlf
o
Wlf
Qtz
p
Wlf
q
Qtz
Wlf
r
Wlf

Figure 6.

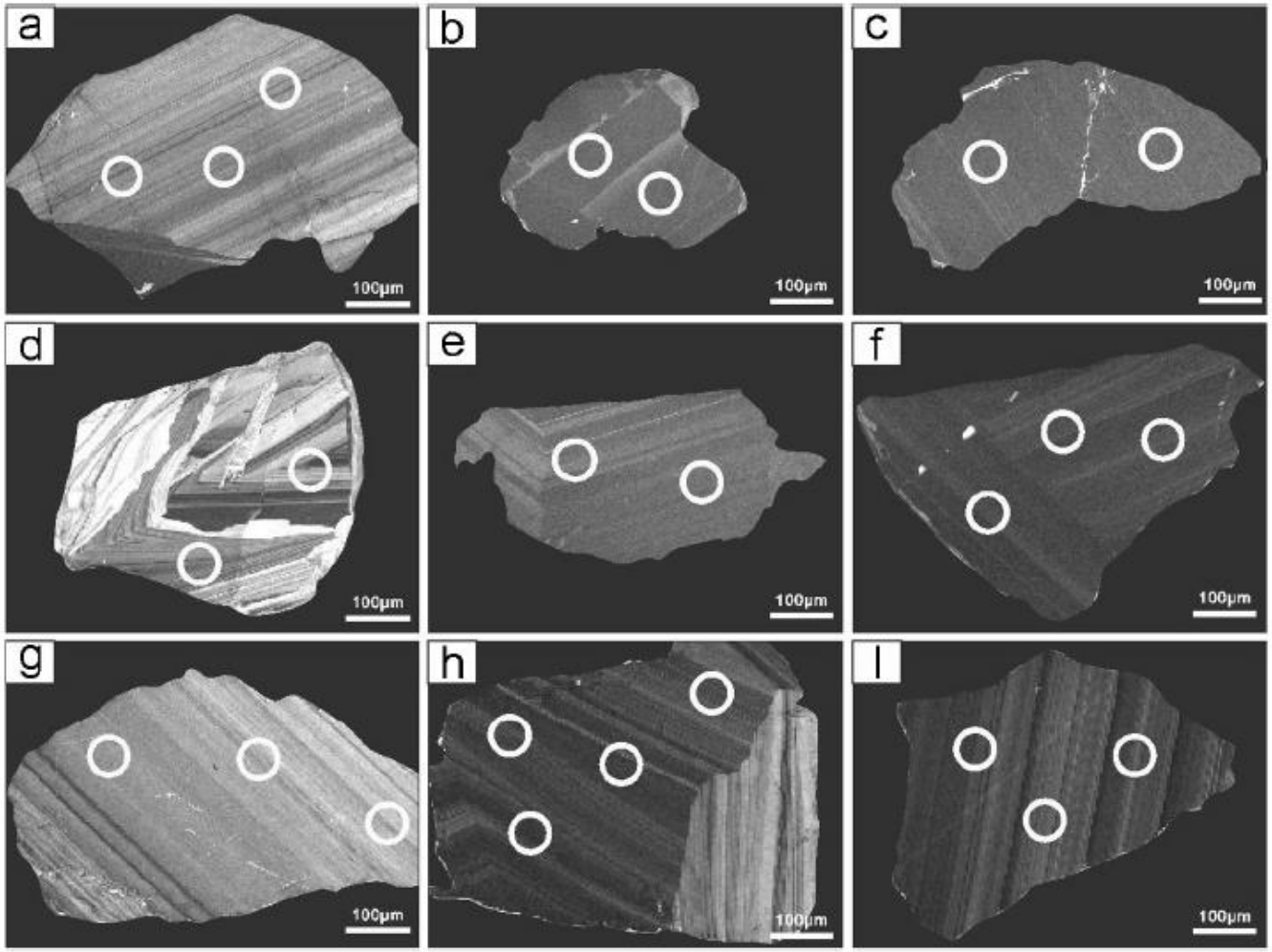
a
100μm
b
100μm
c
100μm
d
100μm
e
100μm
f
100μm
g
100μm
h
100μm
I
100μm

Figure 7.

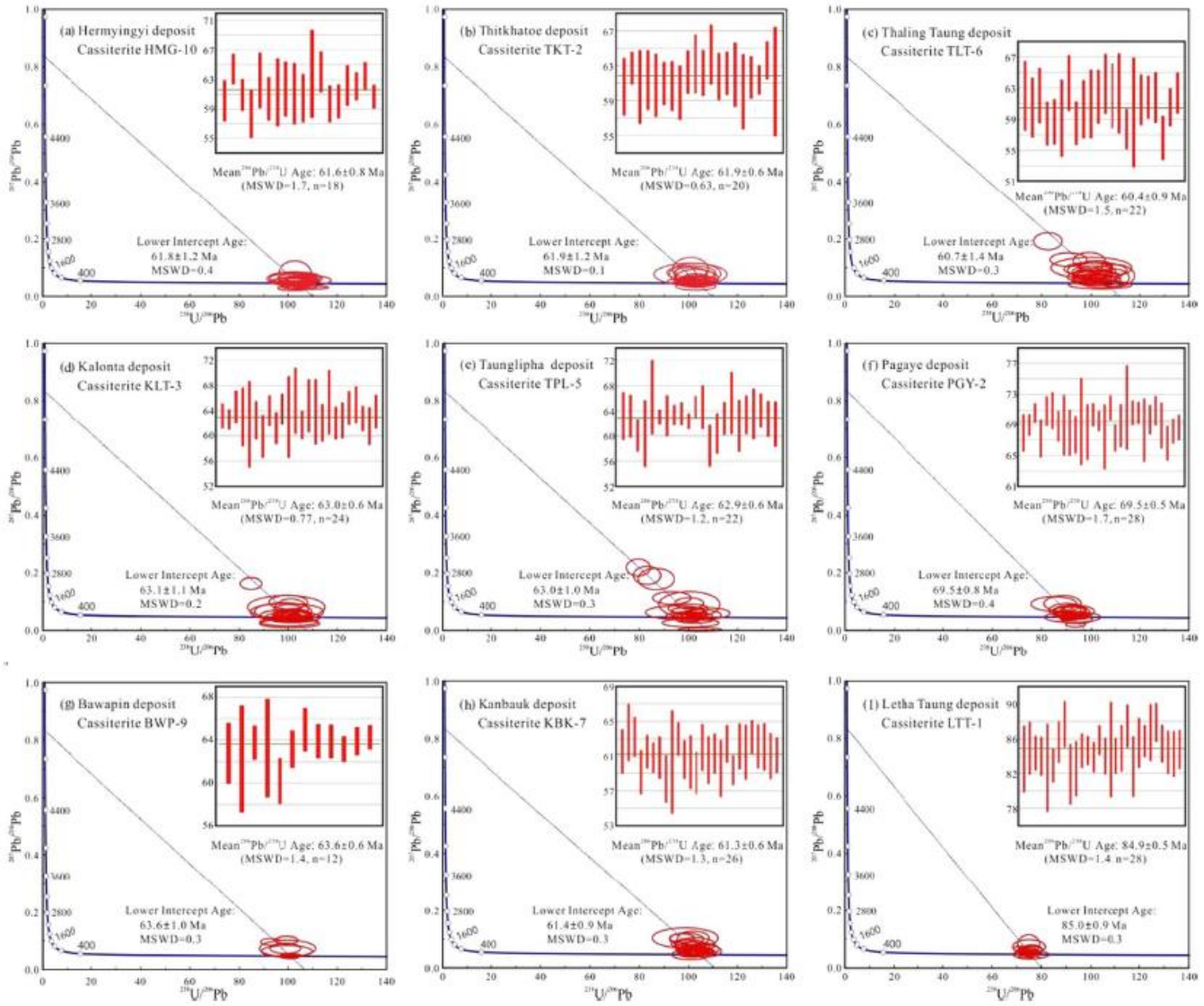
(a) Hermyingyi deposit
Cassiterite HMG-10
Mean 206Pb/238U Age: 61.6±0.8 Ma
(MSWD=1.7, n=18)
Lower Intercept Age:
61.8±1.2 Ma
MSWD=0.4
(b) Thitkhatoe deposit
Cassiterite TKT-2
Mean 206Pb/238U Age: 61.9±0.6 Ma
(MSWD=0.63, n=20)
Lower Intercept Age:
61.9±1.2 Ma
MSWD=0.1
(c) Thaling Taung deposit
Cassiterite TLT-6
Mean 206Pb/238U Age: 60.4±0.9 Ma
(MSWD=1.5, n=22)
Lower Intercept Age:
60.7±1.4 Ma
MSWD=0.3
(d) Kalonta deposit
Cassiterite KLT-3
Mean 206Pb/238U Age: 63.0±0.6 Ma
(MSWD=0.77, n=24)
Lower Intercept Age:
63.1±1.1 Ma
MSWD=0.2
(e) Taunglipha deposit
Cassiterite TPL-5
Mean 206Pb/238U Age: 62.9±0.6 Ma
(MSWD=1.2, n=22)
Lower Intercept Age:
63.0±1.0 Ma
MSWD=0.3
(f) Pagaye deposit
Cassiterite PGY-2
Mean 206Pb/238U Age: 69.5±0.5 Ma
(MSWD=1.7, n=28)
Lower Intercept Age:
69.5±0.8 Ma
MSWD=0.4
(g) Bawapin deposit
Cassiterite BWP-9
Mean 206Pb/238U Age: 63.6±0.6 Ma
(MSWD=1.4, n=12)
Lower Intercept Age:
63.6±1.0 Ma
MSWD=0.3
(h) Kanbauk deposit
Cassiterite KBK-7
Mean 206Pb/238U Age: 61.3±0.6 Ma
(MSWD=1.3, n=26)
Lower Intercept Age:
61.4±0.9 Ma
MSWD=0.3
(i) Letha Taung deposit
Cassiterite LTT-1
Mean 206Pb/238U Age: 84.9±0.5 Ma
(MSWD=1.4 n=28)
Lower Intercept Age:
85.0±0.9 Ma
MSWD=0.3
207Pb/206Pb
238U/206Pb

Figure 8.

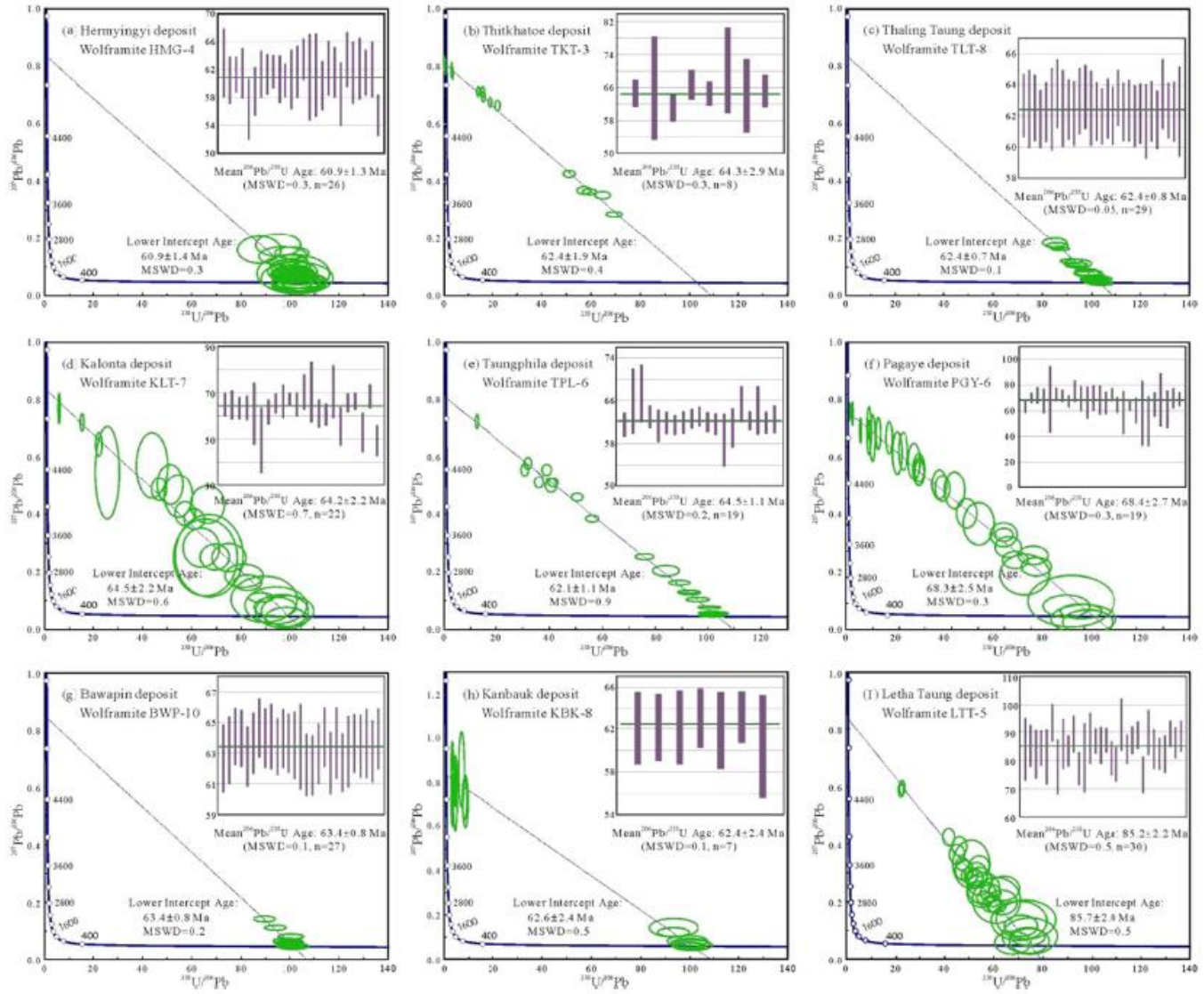
(a) Hermyingyi deposit
Wolframite HMG-4
Mean 206Pb/238U Age: 60.9±1.3 Ma
(MSWD=0.3, n=26)
Lower Intercept Age:
60.9±1.4 Ma
MSWD=0.3
(b) Thitkhatoe deposit
Wolframite TKT-3
Mean 206Pb/238U Age: 64.3±2.9 Ma
(MSWD=0.3, n=8)
Lower Intercept Age:
62.4±1.9 Ma
MSWD=0.4
(c) Thaling Taung deposit
Wolframite TLT-8
Mean 206Pb/238U Age: 62.4±0.8 Ma
(MSWD=0.05, n=29)
Lower Intercept Age:
62.4±0.7 Ma
MSWD=0.1
(d) Kalonta deposit
Wolframite KLT-7
Mean 206Pb/238U Age: 64.2±2.2 Ma
(MSWD=0.7, n=22)
Lower Intercept Age:
64.5±2.2 Ma
MSWD=0.6
(e) Taungphila deposit
Wolframite TPL-6
Mean 206Pb/238U Age: 64.5±1.1 Ma
(MSWD=0.2, n=19)
Lower Intercept Age:
62.1±1.1 Ma
MSWD=0.9
(f) Pagaye deposit
Wolframite PGY-6
Mean 206Pb/238U Age: 68.4±2.7 Ma
(MSWD=0.3, n=19)
Lower Intercept Age:
68.3±2.5 Ma
MSWD=0.3
(g) Bawapin deposit
Wolframite BWP-10
Mean 206Pb/238U Age: 63.4±0.8 Ma
(MSWD=0.1, n=27)
Lower Intercept Age:
63.4±0.8 Ma
MSWD=0.2
(h) Kanbauk deposit
Wolframite KBK-8
Mean 206Pb/238U Age: 62.4±2.4 Ma
(MSWD=0.1, n=7)
Lower Intercept Age:
62.6±2.4 Ma
MSWD=0.5
(I) Letha Taung deposit
Wolframite LTT-5
Mean 206Pb/238U Age: 85.2±2.2 Ma
(MSWD=0.5, n=30)
Lower Intercept Age:
85.7±2.0 Ma
MSWD=0.5
207Pb/206Pb
238U/206Pb

Figure 9.

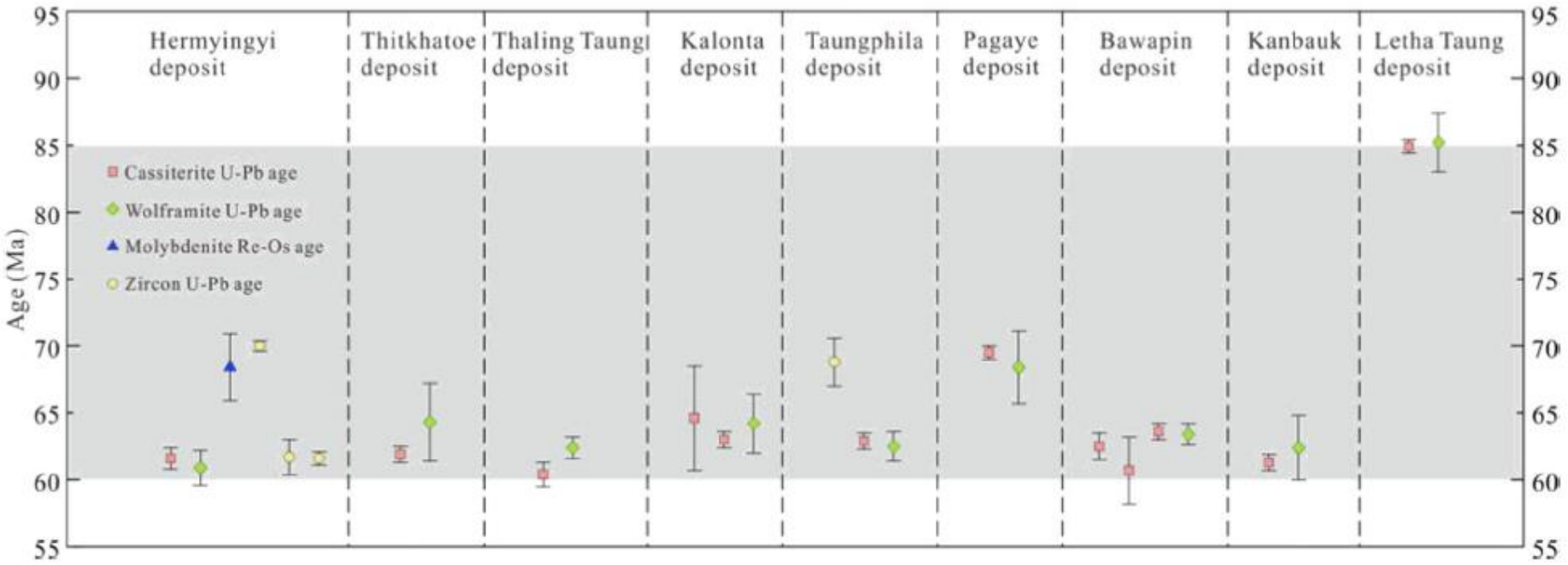
Hermyingyi deposit
Thitkhatoe deposit
Thaling Taungi deposit
Kalonta deposit
Taungphila deposit
Pagaye deposit
Bawapin deposit
Kanbauk deposit
Letha Taung deposit
Cassiterite U-Pb age
Wolframite U-Pb age
Molybdenite Re-Os age
Zircon U-Pb age
Age (Ma)
95
90
85
80
75
70
65
60
55

Figure 10.

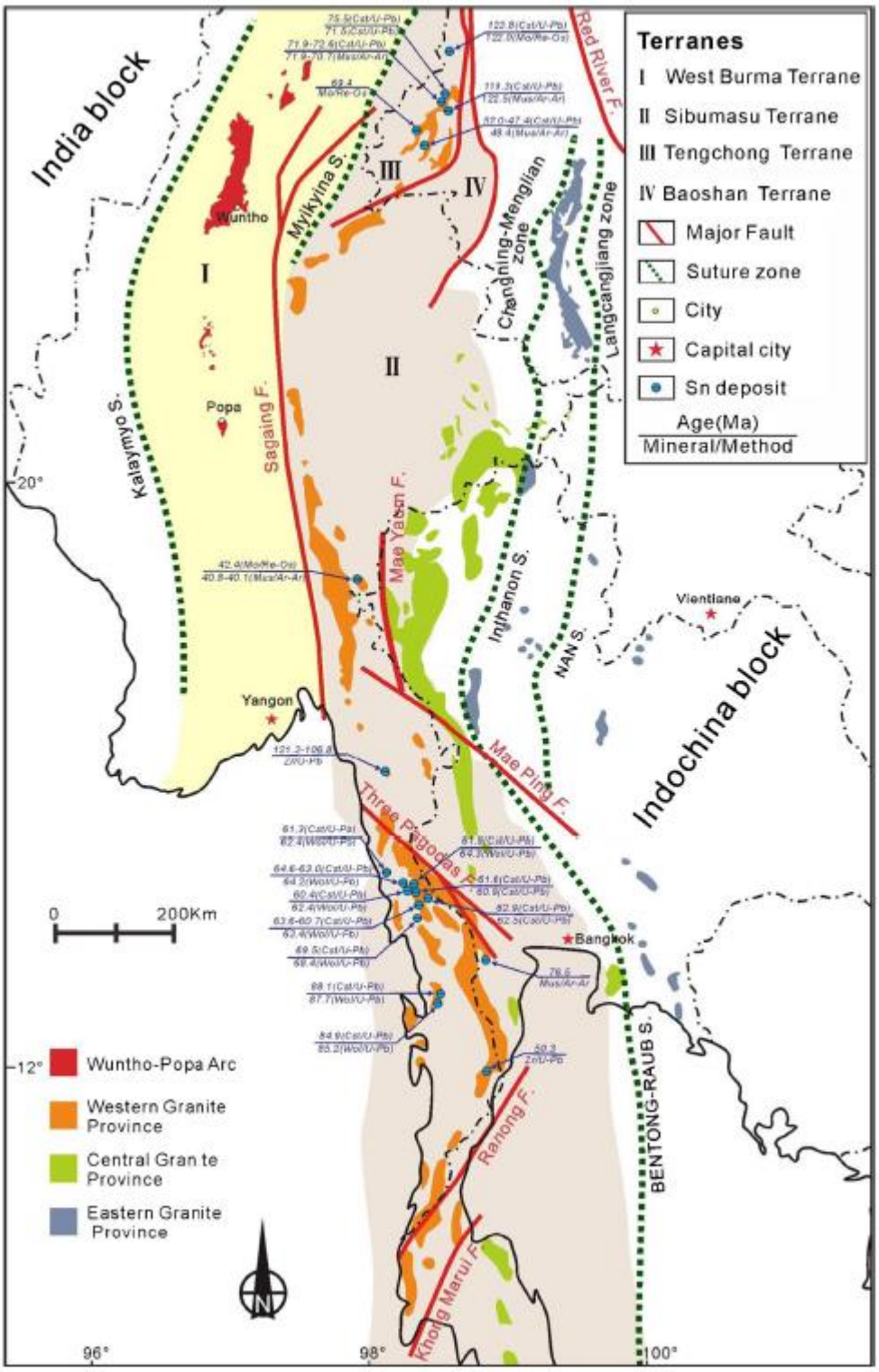
Terranes
I West Burma Terrane
II Sibumasu Terrane
III Tengchong Terrane
IV Baoshan Terrane
Major Fault
Suture zone
City
Capital city
Sn deposit
Age(Ma)
Mineral/Method
India block
Indochina block
Wuntho
Popa
Yangon
Vientiane
Bangkok
Myikyina S.
Sagaing F.
Kalaymyo S.
Chongning-Menglian zone
Langcangjiang zone
Red River F.
Mae Yuam F.
Inthanon S.
NAN S.
Mae Ping F.
Three Pagodas F.
Ranong F.
Khong Marui F.
BENTONG-RAUB S.
0
200Km
Wuntho-Popa Arc
Western Granite Province
Central Gran te Province
Eastern Granite Province
N
20°
12°
96°
98°
100°

Figure 11.

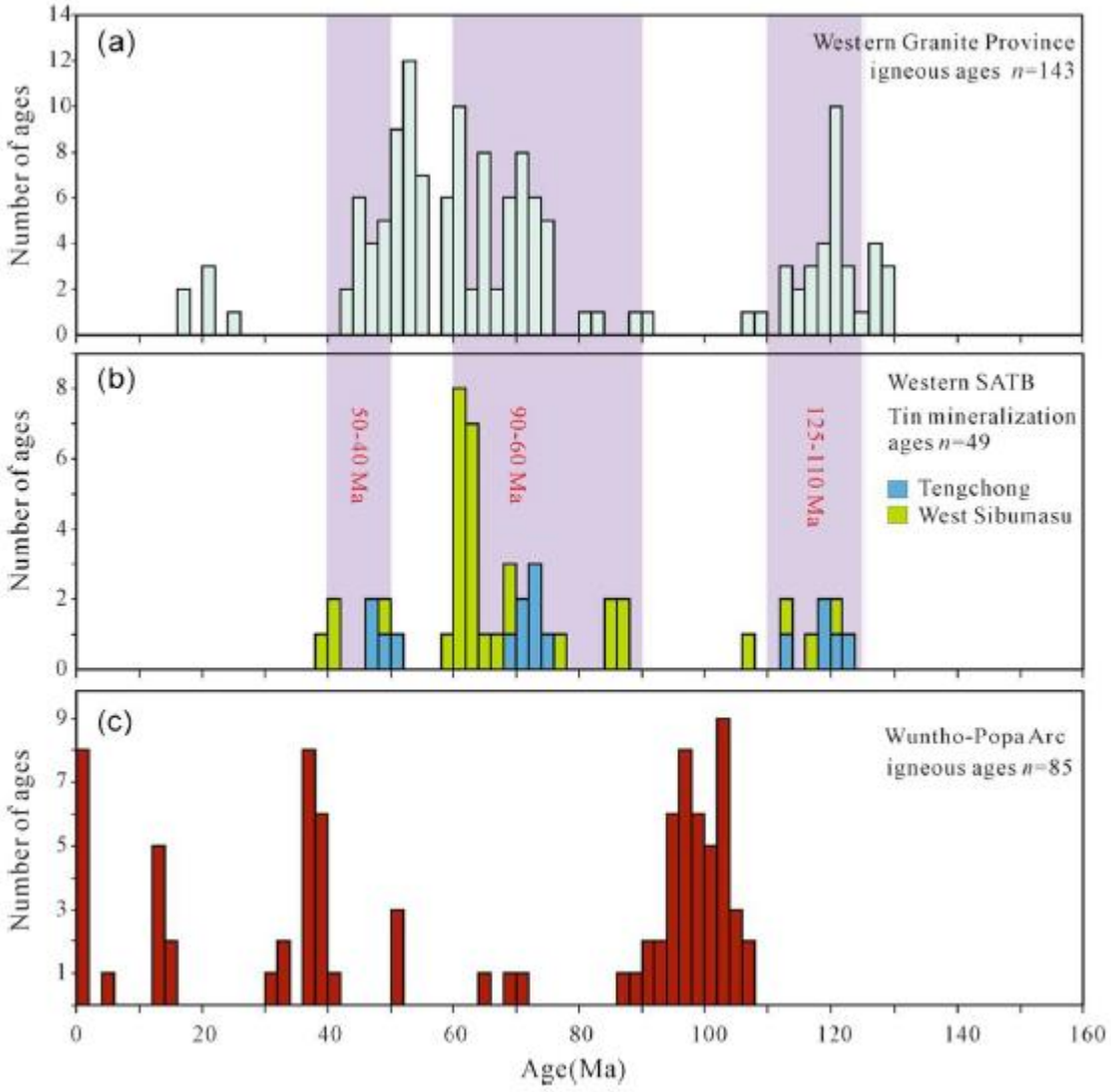
(a)
Western Granite Province
igneous ages n=143
Number of ages
(b)
Western SATB
Tin mineralization
ages n=49
Tengchong
West Sibumasu
50-40 Ma
90-60 Ma
125-110 Ma
Number of ages
(c)
Wuntho-Popa Arc
igneous ages n=85
Number of ages
Age(Ma)

Figure 12.

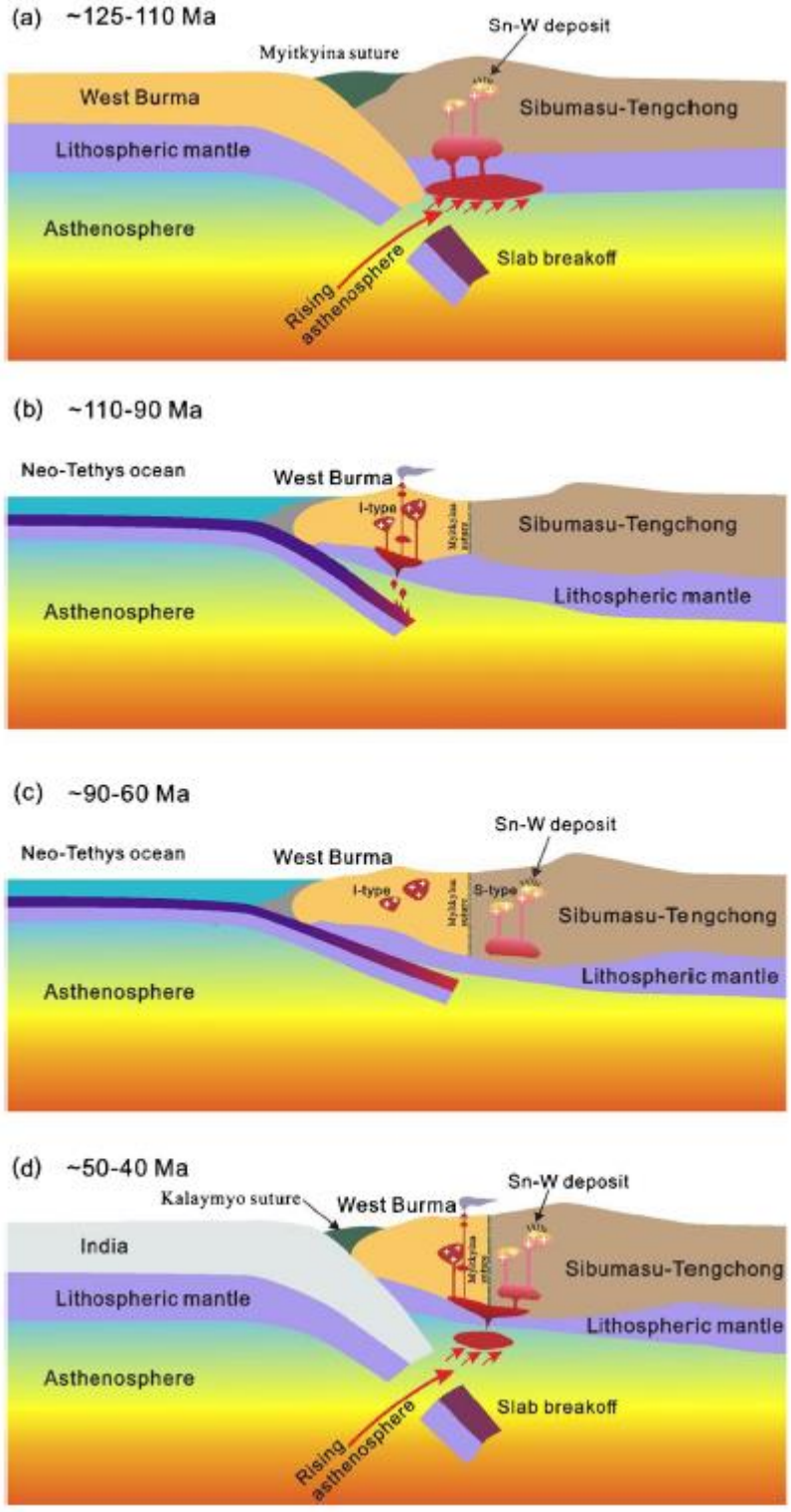
(a) ~125-110 Ma
Sn-W deposit
Myitkyina suture
West Burma
Sibumasu-Tengchong
Lithospheric mantle
Asthenosphere
Slab breakoff
Rising asthenosphere
(b) ~110-90 Ma
Neo-Tethys ocean
West Burma
I-type
Sibumasu-Tengchong
Lithospheric mantle
Asthenosphere
(c) ~90-60 Ma
Sn-W deposit
Neo-Tethys ocean
West Burma
I-type
S-type
Sibumasu-Tengchong
Lithospheric mantle
Asthenosphere
(d) ~50-40 Ma
Kalaymyo suture
West Burma
Sn-W deposit
India
Sibumasu-Tengchong
Lithospheric mantle
Lithospheric mantle
Asthenosphere
Slab breakoff
Rising asthenosphere

Table 1. Information summary of cassiterite and wolframite samples, location and geochronology in this study.

Sample	Mineral	Location	Latitude	Longitude	TW lower intercept age (Ma)	Weighted average ^{207}Pb-corrected $^{206}Pb/^{238}U$ age (Ma)
HMG-10	Cassiterite	Hermyingyi	14°15′	98°21′	61.8 ± 1.2	61.6 ± 0.8
HMG-4	Wolframite				60.9 ± 1.4	60.9 ± 1.3
TKT-2	Cassiterite	Thitkhatoe	14°15′	98°20′	61.9 ± 1.2	61.9 ± 0.6
TKT-3	Wolframite				62.4 ± 1.9	64.3 ± 2.9
TLT-6	Cassiterite	Thaling Taung	14°16′	98°20′	60.7 ± 1.4	60.4 ± 0.9
TLT-8	Wolframite				62.4 ± 0.7	62.4 ± 0.8
KLT-3	Cassiterite	Kalonta	14°17′	98°16′	63.1 ± 1.1	63.0 ± 0.6
KLT-7	Wolframite				64.5 ± 2.2	64.2 ± 2.2
TPL-5	Cassiterite	Taungphila	14°13′	98°21′	63.0 ± 1.0	62.9 ± 0.6
TPL-6	Wolframite				62.1 ± 1.1	62.5 ± 1.1
PGY-2	Cassiterite	Pagaye	14°05′	98°19′	69.5 ± 0.8	69.5 ± 0.5
PGY-6	Wolframite				68.3 ± 2.5	68.4 ± 2.7
BWP-9	Cassiterite	Bawapin	14°09′	98°23′	63.6 ± 1.0	63.6 ± 0.6
BWP-10	Wolframite				63.4 ± 0.8	63.4 ± 0.8
KBK-7	Cassiterite	Kanbauk	14°34′	98°01′	61.4 ± 0.9	61.3 ± 0.6
KBK-8	Wolframite				62.6 ± 2.4	62.4 ± 2.4
LTT-1	Cassiterite	Letha Taung	12°14′	98°59′	85.0 ± 0.9	84.9 ± 0.5
LTT-5	Wolframite				85.7 ± 2.0	85.2 ± 2.2

Table 2. Summary of geological characteristics, zircon U–Pb, and mineralization ages from typical tin deposits in Western SATB

Deposit name	Lat./Long	Deposit type	Associated mag -matic rocks	Zircon U–Pb age (Ma)	Mineralization age (Ma)	Sn + W reserve (tonne)	Reference
Western Sibumasu terrane							
Ma Makhsan	22°55′, 99°00′	Vein/alluvial Type Sn	No data	No data	No data	No data	Htun et al. (2017)
Mawpalaw Taung	15°45′, 97°51′	Vein-type Sn–W	Two–mica granite, pegmatite	121.3–106.8	No data	No data	Paik (2017)
Kuntabin	12°24′, 98°99′	Vein-type Sn–W	Two–mica granite	90.1	88.1, Cassiterite U–Pb; 87.7, Molybdenite Re–Os	No data	Mao et al. (2020)
Letha Taung	12°14′, 98°59′	Vein-type Sn–W	Biotite granite	No data	84.9, Cassiterite U–Pb; 85.2, Wolframite U–Pb	No data	This study
Pilok	14°40′, 98°25′	Vein-type Sn–W	Biotite granite, aplogranite	No data 7	6.5, Muscovite Ar–Ar	50,000	Lehmann et al. (1994)
Pagaye	14°05′, 98°19′	Vein-type Sn–W	Biotite granite	No data	69.5, Cassiterite U–Pb; 68.4, Wolframite U–Pb	6050	This study
Kalonta	14°17′, 98°16′	Vein/alluvial type Sn–W	Biotite granite	No data	64.6–63.0, Cassiterite U–Pb; 64.2, Wolframite U–Pb	No data	Li et al. (2018b); This study
Thitkhatoe	14°15′, 98°20′	Vein-type Sn–W	Biotite granite	No data	61.9, Cassiterite U–Pb, 64.3, Wolframite U–Pb	No data	This study

Table 2 (cont).

Taungphila	14°13′, 98°21′	Vein/greisen type Sn–W	Biotite granite	68.8	62.9, Cassiterite U–Pb, 62.5, Wolframite U–Pb	No data	Jiang et al. (2017); This study
Bawapin	14°09′, 98°23′	Vein-type Sn–W	Biotite granite, garnet–muscovite Granite	No data	63.6–60.7, Cassiterite U–Pb; 63.4, Wolframite U–Pb		No data Li et al. (2018b); This study
Thaling Taung	14°16′, 98°20′	Vein-type Sn–W	Biotite granite	No data	60.4, Cassiterite U–Pb; 62.4, Wolframite U–Pb	No data	This study
Wagone	14°12′, 98°19′	Vein-type Sn–W	Biotite granite	61.4	No data	No data	Li et al. (2018a)
Kanbauk	14°34′, 98°01′	Vein/skarn-type Sn–W	Biotite granite	No data	61.3, Cassiterite U–Pb; 62.4, Wolframite U–Pb	1323	This study
Hermyingyi	14°15′, 98°35′	Vein-type Sn–W	Biotite granite	61.6–70.5	61.6, Cassiterite U–Pb; 68.4, Molybdenite Re–Os; 60.9, Wolframite U–Pb	>2636	Mitchell et al. (2012); Jiang et al. (2017, 2019) Li et al. (2018b); This study
Yadanabon	12°17′, 99°17′	Vein/alluvial type Sn–W	Biotite granite	50.3	No data	43	Gardiner et al. (2016a)
Mawchi	18°45′, 97°10′	Vein-type Sn–W	Biotite granite, Tourmaline Granite	42.0–44.6	42.4, Molybdenite Re–Os; 40.8–40.1 40.8, Muscovite Ar–Ar	102,022	Myint et al. 2017, 2018)
Tengchong terrane							
Jiaojiguan	25°51′, 98°33′	Skarn-type Fe–Sn	Quartz porphyry, Biotite monzonitic	124.1	123.8, Cassiterite U–Pb; 122.0, Molybdenite Re–Os	No data	Cao et al. (2017a)

Table 2 (cont).

Tieyaoshan	25°19′, 98°27′	Skarn-type Sn	Biotite granite	126.0	119.3, Cassiterite U–Pb; 122.5, Muscovite Ar–Ar	No data	Cao et al. (2017a), Chen et al. (2014)
Dasongpo	25°83′, 98°34′	Greisen-type Sn	Biotite granite	75.3–70.3	75.5–71.9, Cassiterite U–Pb	> 1000	Ma et al. (2013) Chen et al. (2014)
Xiaolonghe	25°50′, 98°43′	Vein/greisen type Sn	Biotite granite	76.2–71.4	71.9–72.6, Cassiterite U–Pb; 71.9–70.7, Muscovite Ar–Ar	26,200	Chen et al. (2014); Cao et al. (2016); Wu et al. (2019)
Lailishan	24°83′, 98°22′	Vein/greisen type Sn	Biotite granite, monzogranite	53.0–50.0	52.0–47.4, Cassiterite U–Pb; 48.4, Muscovite Ar–Ar	42,600	Chen et al. (2014); Cao et al. (2017b); Wu et al. (2019)
Xinqi	25°4′, 98°18′	Vein/greisen type Sn	Biotite granite	No data	69.4, Molybdenite Re–Os	No data	Zhou et al. (2017)